A cosmogenic nuclide chronology of Cordilleran Ice Sheet configuration during the Last Glacial Maximum in the northern Alexander Archipelago, Alaska

5   Caleb K. Walcott[1], Jason P. Briner[1], James F. Baichtal[2], Alia J. Lesnek[3], Joseph M. Licciardi[4]

[1]Department of Geology, University at Buffalo, Buffalo, NY 14260, USA

[2]Tongass National Forest, Thorne Bay, AK 99919, USA

[3]School of Earth and Environmental Sciences, CUNY Queens College, Flushing, NY 11367, USA

10 [4]Department of Earth Sciences, University of New Hampshire, Durham, NH 03824, USA

Correspondence to: Caleb K. Walcott (ckwalcot@buffalo.edu)

Abstract

The late-Pleistocene history of the coastal Cordilleran Ice Sheet (CIS) remains relatively

15 unstudied compared to chronologies of the Laurentide Ice Sheet. Yet accurate reconstructions of

CIS extent and timing of ice retreat along the Pacific Coast are essential for a variety of reasons

including paleoclimate modeling, assessing meltwater contribution to the North Pacific, and

determining the availability of ice-free land along the coastal CIS margin for human migration

from Beringia into the Americas. To improve the chronology of CIS history in the Alexander

20 Archipelago, Alaska, we applied [10]Be and [36]Cl dating to boulders and glacially sculpted bedrock

outcrops in areas previously hypothesized to have remained ice-free throughout the local Last

Glacial Maximum (lLGM; 20-17 ka). Results indicate that these sites, and more generally the

coastal northern Alexander Archipelago, became ice-free by 15.1 ± 0.9 ka (n = 12 boulders; 1

SD). We also provide further age constraints on deglaciation along the southern Alexander

25 Archipelago and combine our new ages with data from two previous studies. We determine that

ice retreated from the outer coast of the southern Alexander Archipelago at 16.3 ± 0.8 ka (n = 14

boulders; 1 SD). These results collectively indicate that areas above modern sea level that were previously mapped as glacial refugia were covered by ice during the lLGM until between ~16.3 and 15.1 ka. As no evidence was found for ice-free land during the lLGM, our results suggest

30   that previous ice-sheet reconstructions underestimate the regional maximum CIS extent, and that all ice likely terminated on the continental shelf. Future work should investigate whether presently submerged areas of the continental shelf were ice-free.

1 Introduction

35   The late-Pleistocene history of the coastal Cordilleran Ice Sheet (CIS) remains relatively unstudied compared to chronologies of the Laurentide Ice Sheet (LIS; Dalton et al., 2020). CIS margin reconstructions from the Pacific Coast are based largely on qualitative field observations with little chronologic control (Dyke, 2004; Carrara et al., 2007; Dalton et al., 2020). While a few studies have recently generated local ice sheet retreat chronologies from terrestrial locations

40   along the Pacific Coast (Darvill et al., 2018; Lesnek et al., 2018; Lesnek et al., 2020), there remain vast stretches of the Pacific coastline that lack direct age constraints on deglaciation (Fig. 1). Accurate reconstructions of CIS extent and the timing of ice retreat along the Pacific Coast are essential for paleoclimate modeling, assessing glacial meltwater contributions to the North Pacific and subsequent Northern Hemisphere climate impacts, predicting future mass loss

45   from other marine-terminating ice sheets, and determining whether a coastal route from Beringia into the Americas was viable for humans during southward migration.

        Much of the Northern Hemisphere was covered by continental ice sheets during the global Last Glacial Maximum (gLGM; ~26 – 19 ka). While the LIS and many alpine glaciers worldwide were at their greatest extents during this time, the coastal CIS and the Puget Lobe

50   reached maximum size ~20 – 17 ka (local Last Glacial Maximum; hereafter lLGM; Porter and

Swanson, 1998; Booth et al., 2003; Praetorius and Mix, 2014; Lesnek et al., 2018).

Accurate constraints of CIS deglaciation are necessary to investigate research topics

across numerous disciplines. Recent studies have explored the CIS contributions to meltwater

pulse 1A (~14.6 ka) following the saddle collapse between the LIS and CIS (Gregoire et al.,

55   2016; Ivanovic et al., 2017). Improved constraints on CIS history around meltwater pulse 1A are

necessary to elucidate any influences coastal CIS configuration and retreat had on saddle

collapse. Additionally, numerical modeling studies show differing responses of the CIS to last

deglacial climate oscillations, thus highlighting the need for an improved CIS chronology to

bolster model improvement and validation (Tarasov et al., 2012; Seguinot et al., 2014; Gregoire

60   et al., 2016; Seguinot et al., 2016; Ivanovic et al., 2017). Finally, a temporally accurate

paleogeographic reconstruction of the coastal CIS margin is required to assess whether a viable

coastal route existed for early Americans migrating from Beringia into the Americas. This route

hinges on the presence of ice-free land (refugia) suitable for human habitation throughout the

lLGM. Earlier mapping efforts and other supporting information indicate areas of potential

65   refugia along the former coastal CIS margin (Demboski et al., 1999; Cook et al., 2001; Carrara et

al., 2003; Carrara et al., 2007; Shafer et al., 2010; Shafer et al., 2011).

This study has two goals: 1) to improve the spatio-temporal patterns of coastal CIS

deglaciation in southeastern Alaska (SE AK), and 2) to assess whether areas of the northern

Alexander Archipelago mapped as refugia were ice-free throughout the lLGM and thus available

70   for human habitation (Fig. 2). We report 25 new cosmogenic [10]Be exposure ages from boulders

and bedrock from the northern Alexander Archipelago – the first exposure ages documenting

CIS retreat from the coastal northern Alexander Archipelago. We also report four [10]Be and four

cosmogenic [36]Cl ages from Suemez Island in the southern Alexander Archipelago. Our data

constrain the deglaciation of the marine-terminating CIS margin while expanding the overall

75   North Pacific coastal glacial chronology. Our results suggest deglaciation of coastal regions

~15.4 – 14.8 ka in the northern Alexander Archipelago and do not support previous mapping that

shows refugia in areas that are presently above sea level.

2 Setting

80

The Alexander Archipelago, SE AK, stretches ~480 km (Fig. 2) along the western coast

of British Columbia. The southern part of the archipelago is dominated by Prince of Wales Island

and surrounding islands, whereas the northern part encompasses Baranof and Chichagof Islands

and a collection of smaller islands. The Alexander Archipelago consists of accreted terranes

85   (Cretaceous to Triassic in age) with quartz-bearing diorite and granodiorite units and notable

Eocene-Miocene granitic intrusive complexes (Wilson et al., 2015). Late-Pleistocene volcanic

activity on southern Kruzof Island formed the Mt. Edgecumbe volcanic field (Riehle, 1996).

Post-lLGM (late-Pleistocene and Holocene) eruptions formed extensive andesite flows on the

island and blanketed much of the surrounding area with tephra (Riehle et al., 1984; Riehle et al.,

90   1992; Riehle, 1996). Modern climate of the Alexander Archipelago is dominated by cool, wet

summers and mild winters, with perennial heavy rainfall (Ager, 2019). Snowfall is minimal at

lower elevations, but more substantial in higher elevation areas (https://wrcc.dri.edu/summary/

Climsmak.html). Glaciers occupy alpine cirques in the Alexander Archipelago (totaling < 150

km^2), primarily on Baranof and Chichagof islands (Molnia, 2008). Presently, low-elevation (<

95   700 m asl) areas of the archipelago are dominated by coniferous rain forests, while alpine tundra

exists above the tree line (> 700 m asl; Ager, 2019).

Previous mapping shows much, if not all, of SE AK covered by the CIS during the lLGM

and the last deglaciation, with a maximum position likely terminating several kilometers out on

the continental shelf of the Gulf of Alaska (Carrara et al., 2007). Ice caps formed atop the Coast

100   Mountains and high massifs of the Alexander Archipelago, coalesced, and flowed westward to

the continental shelf and the Pacific Ocean (Capps, 1932; Mann, 1986; Mann and Hamilton,

1995). Outlet glaciers occupied the present fjord and strait landscape (Carrara et al., 2007).

Today, the landscape is strewn with clear indicators of widespread glaciation (deep fjords,

glacially sculpted bedrock draped with boulders, and a variety of other glacial landforms), but it

105   remains unclear whether all of SE AK was covered by the CIS during the lLGM. Some areas of

the Alexander Archipelago, presently above sea level, were mapped as ice-free throughout the

lLGM (Carrara et al., 2007). Recent studies using [10]Be surface exposure dating of glacial

landforms, however, indicate that some of these areas of hypothesized ice-age refugia in the

southern Alexander Archipelago were covered by the CIS during its lLGM advance (Lesnek et

110   al., 2018). Other areas previously interpreted as ice age refugia in the northern Alexander

Archipelago are investigated in this study.

Knowledge of the late-Pleistocene glacial history of the southern Alexander Archipelago

and areas of coastal British Columbia has recently improved. Radiocarbon-dated marine

sediments indicate that the CIS reached its maximum extent sometime between ~25 and ~18 ka

115   in SE AK (Mann and Hamilton, 1995; Barrie and Conway, 1999; Praetorius and Mix, 2014).

Later work, combining ^{14}C dating of terrestrial macrofossils from Shuká Káa and [10]Be dating of

glacial erratics and sculpted bedrock demonstrated maximum CIS extent in the Prince of Wales

Island region between ~19.8 and ~17 ka, followed by rapid retreat between ~17 and 15 ka, leading to ice-free inner fjords and sounds by 15 ka and a transition to a primarily land-

120   terminating ice sheet thereafter (Lesnek et al., 2018; Lesnek et al., 2020; Baichtal et al., in press). A speleothem from Prince of Wales records a growth hiatus from 41.5 ± 0.2 ka to 13.4 ± 0.2 ka, interpreted as the presence of permafrost and/or the CIS over the cave, and thus mean annual air temperatures below 0°C during this time (Wilcox et al., 2019). About 400 km to the south in central coastal British Columbia, CIS deglaciation began ~18.2 ka on Calvert Island, within

125   maximum (~27 ka) and minimum (~16 ka) terrestrial macrofossil ^{14}C age constraints on nearby Haida Gwaii (Warner et al., 1982; Mathewes and Clague, 2017). Records of alkenone-derived sea surface temperatures (SSTs), ice-rafted debris (IRD), and $\delta^{18}O$ from marine sediment cores in the Gulf of Alaska show two periods of increased temperatures and concurrent meltwater input at ~17 ka and ~14.7 ka (Kienast and McKay, 2001; Cosma et al., 2008; Davies et al., 2011;

130   Taylor et al., 2014; Maier et al., 2018). The retreat of the CIS in southeastern Alaska and coastal British Columbia is attributed primarily to this ocean warming and eustatic sea level rise at the CIS margins beyond the zero-meter isobase, potentially exacerbated by atmospheric temperature and precipitation changes (Lesnek et al., 2020).

        Although recent CIS chronologies from the southern Alexander Archipelago provide new

135   insight into the regional glacial history, few direct ages for CIS deglaciation are available elsewhere along the coastal CIS, including the northern Alexander Archipelago. Basal radiocarbon ages from Hummingbird Lake on southwestern Baranof Island indicate regional CIS deglaciation prior to 15.0 ka (Ager, 2019). Tephra overlying IRD in Sitka Sound and draped across Baranof and several other islands is dated to 14.6 ka and provides a minimum constraint

140   on the retreat of marine-terminating margins onto land (Praetorius et al., 2016). Previous

mapping (Carrara et al., 2007; Dalton et al., 2020) shows ice-free coastal terrain currently above sea level during the lLGM; if confirmed with numerical dating techniques, this would be a significant confirmation of the existence of coastal refugia.

3 Methods

3.1 Boulder and bedrock sampling

We collected 29 samples for cosmogenic [10]Be surface exposure dating (hereafter [10]Be dating) during summer 2018, 2019, and 2020 (Figs. 3 and 4). These included 11 bedrock and 18 boulder samples from Suemez (n = 4), Baranof (n = 11), Biorka (n = 4), Kruzof (n = 4) and Chichagof (n = 6) islands. Our samples ranged in elevation from ~50 to ~930 m asl; all sites are above the local marine limits of ~10 – 20 m asl (Baichtal et al., in press). We preferentially sampled paired sites consisting of stable boulders and neighboring unvegetated bedrock surfaces. This allows us to assess whether bedrock surfaces contain isotopic inheritance, which helps interpret our suite of [10]Be ages and provides insights into ice-sheet erosion history. In the absence of suitable boulders at a few locations, we sampled bedrock with clear evidence of glacial erosion to mitigate the possibility of [10]Be inheritance.

We also collected samples from four glacially-transported boulders on the southwestern portion of Suemez Island for [36]Cl surface exposure dating during the summer 2019 field season (Figs. 5; 6; Table 2). The boulders consist of non-vesicular olivine basalt of a similar composition to a Pleistocene-aged basalt flow mapped on southwestern Suemez Island by Eberlein et al. (1983).

Surface samples were collected from the upper few centimeters of the boulders and

165   bedrock using a handheld angle grinder, hammer, and chisel. We avoided sampling areas of the

boulder tops and bedrock surfaces with visible signs of surface erosion (e.g., fractures,

weathering pits). However, we did observe these features elsewhere on the boulders sampled for

[36]Cl dating. We recorded sample locations with a handheld GPS unit or GAIA GPS (both with a

vertical uncertainty of ± 5 m) and measured topographic shielding in the field with a clinometer

170   and compass.

3.2 [10]Be dating

We processed samples at the University at Buffalo Cosmogenic Isotope Laboratory

175   following established quartz purification and beryllium extraction procedures (e.g., Corbett et al.,

2016). After quartz purification, we dissolved samples in hydrofluoric acid with precisely

weighed [9]Be carrier (PRIME Lab 2017.11.17-Be #3/#4; [9]Be concentration of 1074 ± 8 ppm). We

isolated, oxidized, and packed beryllium into target cathodes in five different batches for

accelerator mass spectrometer (AMS) analysis at PRIME lab at Purdue University. The samples

180   were measured with respect to the 07KNSTD standard ([10]Be/[9]Be ratio of 2.85 x 10^{-12}; Nishiizumi

et al., 2007). We corrected sample ratios using batch-specific blank values between 7.50 x 10^{-16}

and 3.14 x 10^{-15}. AMS analytical uncertainty ranged from 3.2 to 7.3% with an average value of

4.7%.

We calculated all [10]Be ages using version 3 of the CRONUS-Earth exposure age

185   calculator (hess.ess.washington.edu; Balco et al., 2008; Balco, 2017), using the Arctic production

rate (Young et al., 2013) and a time-dependent (Lm) scaling scheme (Lal, 1991).

3.3 ^{36}Cl dating

190   All whole rock samples were prepared at the University of New Hampshire Cosmogenic

Isotope Laboratory using a modified version of the protocols in Stone et al. (2000) and Licciardi

et al. (2008). Samples were crushed to a 125-250 μm grain size, then rinsed in deionized water

and leached in a weak HNO_3 solution to remove organic material. Each leached sample was

homogenized using a riffle splitter and a ~1.2 g aliquot was removed to determine total sample

195   chloride. The aliquots were spiked with a small amount of ^{37}Cl-enriched solution (LLNL Spike

A; ^{35}Cl/^{37}Cl = 0.93; 1285 ± 3 ppm Cl). Aliquots also received ~4000 μg of Br (in the form of

NH_4Br), which served to increase the size of the final precipitate. The aliquots were then

dissolved in a solution of HF and HNO_3. After dissolution, fluoride compounds were removed by

centrifuging. Ag(Cl+Br) was precipitated through the addition of $AgNO_3$. The Ag(Cl+Br)

200   precipitates were recovered, rinsed, and packed into stainless steel cathodes for measurement of

^{35}Cl/^{37}Cl ratios, which were used to calculate total sample chloride by isotope dilution methods

(Faure, 1986). For the ^{36}Cl extraction, samples received a small amount of natural-ratio Cl carrier

(^{35}Cl/^{37}Cl = 3.127; 1436 ± 9 ppm Cl) to ensure consistent Cl loads within   the analytical batch.

All samples received ~4800 μg of Br. The samples were dissolved in an HF-HNO_3 solution and

205   insoluble fluorides were removed through centrifuging. Ag(Cl+Br) was precipitated by adding

$AgNO_3$. The Ag(Cl+Br) precipitates were recovered and dissolved in a solution of NH_4OH. To

remove ^{36}S, an isobar of ^{36}Cl, $BaNO_3$ was added to the solutions to precipitate $BaSO_4$. The

purified Ag(Cl+Br) was precipitated by acidifying the solutions with HNO_3 and adding $AgNO_3$.

The Ag(Cl+Br) precipitates were then recovered, rinsed, and dried.

210   ^{35}Cl/^{37}Cl and ^{36}Cl/Cl ratios were measured at the Center for Accelerator Mass

Spectrometry at Lawrence Livermore National Laboratory. Analytical uncertainty on ^{35}Cl/^{37}Cl

measurements ranged from 0.04% to 0.43%; analytical uncertainty on [36]Cl/Cl measurements

ranged from 2.12% to 2.87%. Major and trace element analyses were conducted by SGS

Minerals Services in Burnaby, British Columbia, Canada. Reported total Cl and [36]Cl

215   concentrations are corrected for process blanks (Table 2). Analytical data used to determine

surface exposure ages are provided in supplementary tables S1 and S2. [36]Cl exposure ages were

calculated using an in-development version of the CRONUS-Earth [36]Cl calculator

(http://stoneage.ice-d.org/math/Cl36/v3/v3_Cl36_age_in.html) and Lm scaling (Lal, 1991). For

comparison, [36]Cl ages calculated using version 2.1 of CRONUScalc (Marrero et al., 2016a) are

220   included in supplementary table S3.

3.4 Exposure age calculation considerations

We made no corrections for post-glacial elevation changes, post-depositional erosion, or

225   snow cover when calculating our [10]Be and [36]Cl ages. Post-glacial isostatic adjustment results in a

time-varying rate of cosmogenic nuclide production (Jones et al., 2019). This can be corrected

for using comprehensive records of regional emergence constrained by glacier isostatic

adjustment models or relative sea level histories. Hundreds of radiocarbon ages constrain the

relative sea level chronology in the Alexander Archipelago; the sites in our study experienced

230   ~50 m of relative sea level lowering due to forebulge collapse between ~15 and 10 ka (Baichtal

et al., in press). Corrections for this, albeit slightly uncertain given site-to-site differences in

elevation history, result in small changes (~1% age decrease), and thus we report our ages

without any correction for isostatic adjustment (Tables 1 and 2). Furthermore, changes in air

pressure near a retreating ice margin and shifts in air compression above a sample site that

235   experienced elevation change may mitigate any effects of isostatic adjustment on cosmogenic

nuclide production, potentially rendering any elevation correction unnecessary (Staiger et al., 2007).

Post-depositional weathering and erosion can also affect exposure ages. We observed fresh, unweathered glacially scoured bedrock across all our field sites, indicating minimal post-

240   glacial erosion. Therefore, we made no corrections for erosion in our age calculations.

Extended periods of thick and dense snow cover can also inhibit ^{10}Be and ^{36}Cl production in a rock surface and lead to erroneously young apparent exposure ages. While modern snowfall reports for lower-elevation areas of the Alexander Archipelago indicate minimal average wintertime snow cover (10 – 20 cm; https://wrcc.dri.edu/summary/ Climsmak.html), there are no

245   data for higher-elevation areas. Consequently, we cannot report our ages with reliable snow shielding corrections and these exposure dates should be considered minimum ages. However, most of our sites are from low to moderate elevations (<500 m asl; Table 1).

4 Results

250

We sampled from the summit of a massif at ~410 m asl on south-central Suemez Island (southern Alexander Archipelago) and from a flat bench scattered with boulders on the summit's flank for ^{10}Be dating (Fig. 6). The two boulders sampled on the bench date to 15.6 ± 0.7 (19SEAK-07; Fig. 3) and 15.0 ± 1.1 ka (19SEAK-08; we report all surface exposure ages with 1

255   σ internal uncertainty; Table 1.). The summit site featured fresh glacially sculpted bedrock surfaces with a couple boulders resting on the bedrock. A boulder and its adjacent bedrock surface, as a pair, date to 17.4 ± 1.2 (19SEAK-09) and 19.7 ± 1.2 ka (19SEAK-10), respectively (Fig. 3). The three boulders yield a mean age of 16.0 ± 1.2 ka (n = 3; 1 SD).

On southwestern Suemez Island, we sampled four large boulders for ^{36}Cl dating. The

260   boulders were distributed across a terrain of patchy muskeg with locally outcropping bedrock.

Based on reconstructed CIS flow directions (Lesnek et al., 2020) and boulder composition

(supplementary table S2; Eberlein et al., 1983), the boulders were likely plucked from basalt

flows present on the southwestern portion of Suemez Island (Brew, 1996). The four basalt

boulders from southwestern Suemez Island have ^{36}Cl exposure ages ranging from 12.5 ± 1.1 to

265   16.6 ± 1.6 ka (ages are reported at 1 σ internal uncertainty; Fig. 5; Table 2).

We collected samples from four sites (Baranof Sites A – D; Fig. 7) on the ocean-facing

side of Baranof Island, northern Alexander Archipelago. Here, we chose our helicopter ground

stops in an area previously mapped as ice-free throughout the lLGM (Carrara et al., 2007; Fig.

7). Evidence for glacial sculpting of bedrock surfaces is clear; glacial grooves, striations and

270   chatter marks are present at all sites, and the bedrock surfaces, in places, are topped by perched

boulders (Fig. 3). Field evidence of recent glaciation, including relatively unweathered chatter

marks, grooves, and striations, contradicts prior mapping of these areas being ice-free during the

lLGM.

Baranof Site A is a large, unforested area of bedrock outcrops composed of several

275   smaller ridges. Here, we sampled two bedrock surfaces – one from the stoss side of a bedrock

outcrop (19SEAK-18; Fig. 3) and one from the top surface of a nearby bedrock patch (19SEAK-

19) – which date to 21.7 ± 0.9 and 28.0 ± 1.1 ka, respectively. A boulder sampled adjacent to

bedrock (sample 19SEAK-18) yielded an exposure age of 16.9 ± 0.8 ka (19SEAK-17). A second

boulder sample from this stop dates to 14.4 ± 0.7 ka (19SEAK-20; Fig. 3). At Baranof Site B – a

280   raised bedrock knob – we sampled two boulders and one bedrock surface. The two boulders have

^{10}Be ages of 15.1 ± 0.6 ka (19SEAK-23; Fig. 3), 14.4 ± 0.7 ka (19SEAK-21); the bedrock

samples has a ^{10}Be age of 14.4 ± 0.6 ka (19SEAK-22). Baranof Site C is a high ridge between the ocean and a U-shaped valley with abundant bedrock outcrops and few boulders. Here, a boulder yielded an exposure age of 16.3 ± 0.6 ka (19SEAK-24; Fig. 3) whereas a bedrock surface dates to

285   15.7 ± 0.6 ka (19SEAK-25). Finally, Baranof Site D is a small bedrock ridge between two peaks with massive stoss and lee features. At this site, we collected samples from two quartz veins in the bedrock, which have exposure ages of 18.2 ± 0.7 (19SEAK-26; Fig. 3) and 20.2 ± 0.8 ka (19SEAK-27). Because the sites are all in relatively close proximity and from similar elevations (50 – 160 m asl), we treat the samples as having experienced the same glacial history, and thus

290   should belong to a single age population. Collectively, boulder samples yield a mean age of 15.4 ± 1.1 ka (n = 5; 1 SD) with no obvious outliers, whereas the bedrock samples exhibit more scatter and are mostly older than the mean boulder age (Fig. 9).

Biorka Island, a small island off the western coast of central Baranof Island, was initially mapped as ice-covered throughout the lLGM (Dyke, 2004). Here, there are numerous ~1 m tall

295   boulders that rise above the surrounding vegetation and rest on ice-sculpted bedrock. Vegetation and sediments mostly obscure underlying bedrock surfaces, and thus we only collected samples from boulders at this sampling site. Our four boulder samples yielded exposure ages of 15.3 ± 0.5 (18JB005; Fig. 4), 14.9 ± 0.6 (18JB006), 15.4 ± 0.5 (18JB007; Fig. 4), and 13.7 ± 0.5 ka 18JB008), with a mean of 14.8 ± 0.8 ka (n = 4; 1 SD; Fig. 8).

300   We visited a summit ridge at 545 – 560 m asl on the western, ocean-facing side of northwestern Kruzof Island, previously mapped as ice-free throughout the LGM (Dalton et al., 2020). There, we found many large stable boulders and exposed patches of glacially sculpted bedrock between vegetation exhibiting glacial grooves and chatter marks. Here, we sampled three large boulders (> 2 x 2 x 1 m), which date to 14.9 ± 0.8 (20SEAK-07; Fig. 4), 14.9 ± 0.9

305   (20SEAK-12) and 14.6 ± 0.8 ka (20SEAK-13; Fig. 4), yielding a mean age of 14.8 ± 0.2 ka (n =

3; 1 SD; Fig. 8). A bedrock surface at this site dates to 13.4 ± 1.0 ka (20SEAK-10; Fig. 4) and

sits ~10 m below and ~10 m away from the boulder that dated to 14.6 ± 0.8 ka (20SEAK-13).

We collected samples from three sites on Chichagof Island (Chichagof Sites A – C; Fig.

8). Unlike our other sampling locations which are on the ocean-facing, western sides of the

310   archipelago, the Chichagof Island sites are all located inland. We visited these sites to determine

the timing of ice retreat inland and to complement the findings of a previous study that

documented ice withdrawal in the central and eastern Alexander Archipelago (Lesnek et al.,

2020). Chichagof Island is notable for its relative lack of boulders – consequently, the boulders

sampled here are smaller than those at other sites. While many bedrock outcrops featured smooth

315   surfaces indicative of glacial erosion, we did not observe clear striations or chatter marks. At site

A, a bedrock bench, [10]Be ages from two small, perched boulders are 12.7 ± 0.7 (20SEAK-15; 0.5

x 0.3 x 0.3 m; 476 m asl; Fig. 4) and 9.0 ± 0.6 ka (20SEAK-16; 0.5 x 0.4 x 0.3 m; 473 m asl). A

quartz vein sampled from bedrock outcrop at this site has an exposure age of 15.3 ± 0.7 ka

(20SEAK-14). Site B is a series of bedrock ridges, and a single boulder yields an exposure age of

320   12.4 ± 0.9 ka (20SEAK-18; 817 m asl; Fig. 4), while an adjacent bedrock surface dates to 14.1 ±

0.7 ka (20SEAK-19; 816 m asl). Finally, site C is at the summit of a massif and one bedrock

knob sampled here has an exposure age of 17.7 ± 0.8 ka (20SEAK-22; 779 m asl; Fig. 4).

5 Discussion

325

5.1 Bedrock [10]Be ages

We sampled large and stable boulders in addition to bedrock surfaces with clear evidence of

glacial erosion (e.g., striations, chatter marks) with the goal of providing optimal constraints on

330   deglaciation. Sampling bedrock surfaces also allows us to better understand the subglacial

erosion regime across the Alexander Archipelago, potentially yielding information about the

duration of ice cover, the amount of subglacial erosion, and the likelihood of boulders containing

inheritance.

Bedrock exposure ages are older than the mean boulder exposure ages by two SD or

335   greater on Suemez Island (19SEAK-10) and Baranof sites A (19SEAK-18, 19SEAK-19) and D

(19SEAK26, 19SEAK-27). At Chichagof site A the bedrock exposure age (20SEAK-14) is ~4.5

kyr older than the mean boulder age, but still within two standard deviations, perhaps due to the

large spread in boulder ages resulting in larger standard deviations. At Chichagof site B, the

single boulder [10]Be age (20SEAK-18) post-dates the single bedrock age by ~1.7 kyr. In general,

340   bedrock data reported here are consistent with bedrock [10]Be ages from Warren and Baker islands

that are older (by more than 2 SD) than mean boulder ages (Lesnek et al., 2018). Bedrock ages

may be erroneously older due to [10]Be inheritance if ice sheet erosion was insufficient to remove

the ~2 m of rock required to remove most of the previous [10]Be inventory. Studies from British

Columbia (Darvill et al., 2018) and Washington (Briner and Swanson, 1998) also report

345   cosmogenic nuclide inheritance in bedrock from other areas covered by the CIS. In our field

area, the short-lived nature of the overriding event (~3 kyr; Lesnek et al., 2018) may also

contribute to the lack of significant glacial erosion. Finally, traces of inheritance may be present

in bedrock, perhaps even boulders, in ice-sheet-distal sites like these that are overrun by ice

during extremely brief portions of the Quaternary (Briner et al., 2016).

350   In some cases, boulder-bedrock pairs have similar exposure ages (on southern Baranof

and Suemez islands), suggesting our bedrock ages are unaffected by [10]Be inheritance at these

sites. On Kruzof Island, a bedrock patch yields an exposure age that is younger (by more than 2

σ) than the mean age of the surrounding boulders. Potential cover by snow, sediment, or vegetation is thought to have caused anomalously young ages elsewhere in the Alexander

355   Archipelago (Lesnek et al., 2020) and may also explain this [10]Be age from our bedrock site on Kruzof Island.

Bedrock exposure ages vary greatly (by as much as ~14 kyr) between the various sampling locations on Baranof Island and up to 6 kyr on Suemez Island (Lesnek et al., 2018). The Alexander Archipelago is characterized by impressive relief (deep fjords, high peaks), and

360   thus, sub-glacial erosion rates clearly varied greatly across Suemez and Baranof islands where sampling locations are ~2 – 6 km apart. Differing bedrock [10]Be ages from the same sampling locales confirm this, reflecting variable sub-glacial erosion rates even within ~100 m of each other. Some samples may have been collected in areas dominated by glacial abrasion, whereas other samples might be from surfaces dominated by quarrying, and thus, this variability could

365   reflect varying subglacial processes on a local scale.

Because bedrock exposure ages from the coastal Alexander Archipelago (this study; Lesnek et al., 2018) do not consistently pre-date, match, or post-date exposure ages from adjacent boulders, we refrain from including bedrock-based [10]Be ages in our mean age calculations (Figs. 9; 10). This negates biases when choosing which bedrock ages "match"

370   nearby erratic ages and allows us to eliminate any concern over inheritance or post-ice retreat cover of these bedrock surfaces. While bedrock ages, especially when paired with boulder ages, are useful for identifying spatially variable subglacial erosion processes and issues with past cover and inheritance, they do not provide reliable age constraints on the timing of deglaciation. In light of this, we also recalculate relevant mean ages from Lesnek et al. (2018; 2020) using

375   solely boulder [10]Be ages to update these other regional chronologies.

5.2 ^{10}Be chronology incompatible with mapped Cordilleran Ice Sheet extent

We targeted areas of the northern Alexander Archipelago mapped as ice-free by previous studies to determine whether these areas were lLGM refugia. The most recent coastal CIS

380 reconstructions show significant portions of the northern Alexander Archipelago as remaining ice-free throughout the lLGM (Fig. 2), with ice terminating close to the present shoreline – not on the continental shelf (Dalton et al., 2020; Lesnek et al., 2020). Our data, however, indicate that at least some of these areas that were mapped as refugia (southwestern Baranof and Kruzof islands) were covered by ice, and deglaciated around 15.4 – 14.8 ka. Our new evidence thus

385 suggests that ice extended onto the continental shelf during the lLGM, as in the southern Alexander Archipelago (Lesnek et al., 2018). These discrepancies between previously mapped ice extents and those implied by our new exposure ages highlight the need to develop deglaciation chronologies elsewhere along the CIS coastal margin to provide updated mapping around the north Pacific.

390

5.3 Cordilleran Ice Sheet retreat across the Alexander Archipelago

Mean boulder ^{10}Be exposure ages from Suemez Island in this study and Lesnek et al. (2018), 16.0 ± 1.2 ka (n = 3 boulders; 1 SD) and 16.6 ± 0.8 ka (n = 3 boulders; 1 SD), overlap

395 within 1 standard deviation (Figs. 6; 9). However, three of the boulder ^{36}Cl ages from southwestern Suemez Island do not overlap with the ^{10}Be ages, at 1 standard deviation (Figs. 6; 9). We attribute this scatter to post-depositional surface erosion of the boulders. Surface erosion of rocks with low concentrations of native Cl (supplementary table S2), where the primary ^{36}Cl production pathway is Ca-spallation (Marrero et al., 2016b), results in exposure ages that are

400 erroneously young. Thus, we interpret the oldest ^{36}Cl exposure age (16.6 ± 0.5 ka; 19SEAK-02)

as the closest constraint on deglaciation at that site. This ^{36}Cl age overlaps with the ^{10}Be ages

from elsewhere on Suemez Island; we combine them and calculate a new, boulder-based mean

deglaciation age of 16.3 ± 0.8 ka (n = 10 boulders; 1 SD) for Suemez Island.

We group together three of our sampling locations in the northern Alexander Archipelago

405 that are ocean-facing: Kruzof, Biorka, and southern Baranof islands. As the CIS retreated from

the continental shelf inland, these were the first areas presently above sea level to become ice-

free. We calculate a mean ^{10}Be boulder age of 15.1 ± 0.9 ka (n = 12 boulders; 1 SD) for the

coastal northern Alexander Archipelago.

There are limited data from elsewhere in the northern Alexander Archipelago that

410 constrain the timing of deglaciation. A basal pollen concentrate-based radiocarbon age from

Hummingbird Lake (Fig. 7), southwestern Baranof Island dates to 15.0 ± 0.2 ka, in agreement

with the ^{10}Be ages presented here and that collectively indicate coastal Baranof Island was

deglaciated prior to this (Ager, 2019). Additionally, tephra layers from Mt. Edgecumbe on

Kruzof Island are dated to 13.1 ka (Riehle et al., 1992; Beget et al., 1998), and blanket many of

415 the surrounding islands, suggesting that these areas were ice-free by then.

All three sample sites on Chichagof Island (Sites A – C) are not ocean-adjacent and

characterized by a general lack of boulders. The boulders present were much smaller, and

notably, shorter (< 0.5 m high) than boulders sampled elsewhere across the Alexander

Archipelago – we chose to sample these despite their size to provide minimum ages for

420 deglaciation and to compare with available radio carbon constraints. They date between 9.0 ± 0.6

and 12.7 ± 0.7 ka. Their ages are younger than other age constraints for deglaciation on

Chichagof Island; radiocarbon ages on shells from raised marine terraces on Chichagof Island

date back to 14.2 ± 0.6 cal ka suggesting that the island was ice-free by this time (Baichtal et al.,
in press). Smaller boulders are more susceptible to cover (whether snow, vegetation, or

425   sediment), and may thus yield anomalously young [10]Be ages. While a lack of large boulders
found on Chichagof Island make it difficult to ascertain the timing of deglaciation, regional
glacial and sea level history suggests Chichagof Island was deglaciated between 15.1 (when the
coastal area deglaciated) and 14.2 ka (the age of shells in raised marine deposits). Therefore, our
boulders likely have anomalously young exposure ages.

430   Our mean [10]Be age from all sites along the coastal portion of the northern Alexander
Archipelago of 15.1 ± 0.9 ka (n = 12 boulders; 1 SD) fits with the few other regional deglaciation
constraints (Fig. 2) and overlaps within one standard deviation with the mean boulder exposure
age from the southern Alexander Archipelago of 16.3 ± 0.8 ka (n = 13 boulders; 1 σ; this study;
Lesnek et al., 2018; Lesnek et al., 2020).

435   While mean ages from the northern and southern Alexander Archipelago overlap within
one standard deviation, it is possible that these areas deglaciated at slightly different times as
these various sampling sites happened to become ice-free. Furthermore, local ice caps formed
and radiated from massifs on Chichagof, Baranof, and Prince of Wales islands during the lLGM
(Capps, 1932; Mann and Hamilton, 1995; Lesnek et al., 2020). These local ice caps served as a

440   local ice source for the Alexander Archipelago and their locations and flow patterns may have
led to some parts of the archipelago becoming ice-free before others. Thus, we present a range of
deglaciation across the coastal Alexander Archipelago from between 16.3 ± 0.8 ka and 15.1 ±
0.9 ka

Ice retreat across the Alexander Archipelago is also registered in marine sediments off

445   the former coastal CIS margin. Several marine sedimentary records (cores EW0408-26JC,

EW0408-66JC, EW0408-85JC) extending back to ~18.5 cal ka show the presence of IRD beginning ~18.5 ka, peaking at 17.5 – 16.5 ka and ceasing at 14.8 ka, reflecting a final retreat of marine-terminating ice (Praetorius and Mix, 2014). Furthermore, these IRD data record fluctuating but relatively elevated calving spanning 18.5 to 14.8 ka, perhaps indicating steady

450 retreat punctuated by periods of accelerated melting.

Tephra from Mt. Edgecumbe (Kruzof Island) found in core EW0408-26JC is interpreted as being deposited in a submarine environment, suggesting that this core site was ice-free by 14.6 ka (Praetorius et al., 2016). Records of a subsequent eruption dated to ~13.1 cal ka from marine sediments in Sitka Sound (core EW0408-40JC) indicate that this area (between Baranof

455 and Kruzof islands) must have been ice-free by this time (Addison et al., 2010). Finally, ^{14}C ages from mollusks found in a diamicton layer along the Gastineau Channel date to ~13.8 cal ka, reflecting the beginning of deglaciation near the mainland (Miller, 1973; we calibrate all uncalibrated ^{14}C ages with CALIB 8.2; Stuiver et al., 2021).

460 **5.4 Chronologies of Cordilleran Ice Sheet deglaciation across the North Pacific**

Radiocarbon ages from the CIS margin reflect ice advance from ~20 – 17 ka, near the end of the gLGM at 19 ka. Dates from mammalian fossils in Shuká Káa on Prince of Wales Island indicate CIS advance ~20 ka in the Alexander Archipelago (Lesnek et al., 2018). Directly south of the

465 Alexander Archipelago, on eastern Graham Island (Haida Gwaii) initial ice advance is dated to 24.1 – 22.5 cal ka with a ^{14}C date from a twig underlying glacial till (Blaise et al., 1990; Mathewes and Clague, 2017). Along the southwestern CIS margin, ice reached its maximum extent until ~18.3 ka in the Coquitlam Valley and ~17.0 ka in the Puget Sound area (Clague et al., 1980; Porter and Swanson, 1998).

470   Glacier chronologies from the northeastern Pacific coastline also reflect post-gLGM

retreat. On Sanak Island, tephra near the bottom of a lake sediment core dates deglaciation before

~15.9 ka, prior to the onset of CIS withdrawal in the Alexander Archipelago (Misarti et al.,

2012). On Kodiak Island, final lLGM retreat dates to ~15.7 cal ka, as marked by a ^{14}C age above

glacio-tectonically altered sediments (Mann and Peteet, 1994). Directly north of the Alexander

475   Archipelago, a ^{14}C age from a log found within the Finger Glacier lateral moraine provides a

minimum constraint on deglaciation at ~14.6 cal ka (Mann, 1986). Radiocarbon ages from a

marine sediment core in Dixon Entrance date maximum CIS extent to before ~16.1 cal ka and

retreat beginning before ~15.3 cal ka (Barrie and Conway, 1999). A marine sediment record

from Vancouver Sound similarly dates maximum ice extent to 18.5 ka and retreat of the CIS

480   onto the mainland by 16.4 ka (Blaise et al., 1990). Quaternary sediments on eastern Graham

Island indicate the CIS was retreating by 17.8 cal ka (Blaise et al., 1990). Notably, [10]Be ages on

Calvert Island suggest ice retreated off the continental shelf at ~18 ka, pre-dating ice withdrawal

onto land in the Alexander Archipelago (Darvill et al., 2018).

        Marine sediment cores are interpreted to show ice retreat across the coastal northeastern

485   Pacific. A marine sediment core (SO202-27-6) from the Gulf of Alaska captures a decrease in

sea surface salinity ~16 ka, interpreted to reflect increased meltwater from the CIS margin

(Maier et al., 2018). Another marine sediment core (EW0408-85JC) from off the coast of

southern Alaska records a decrease in glacial-margin sediment accumulation at 16.9 ka as ice

stagnated or began to retreat. (Davies et al., 2011). Reductions in salinity captured by planktonic

490    $\delta^{18}O$ in this core at ~16.7 ka are interpreted as an increase in meltwater input from retreating

glaciers. A transition from ice-proximal to laminated hemipelagic sediments at ~14.8 ka marks

glacier retreat off the continental shelf and onto land. Additionally, a marine sediment core from

off Vancouver Island (MD02-2496) captures IRD deposition between ~17.0 and ~16.2 cal ka – indicating rapid regional deglaciation – and a minor IRD event at ~14.7 cal ka (Cosma et al.,

495   2008).

Our new data showing ice retreat at 15.1 ± 0.9 ka from the northern Alexander Archipelago, along with ages of deglaciation from the southern Alexander Archipelago (16.3 ± 0.8 ka; this study; Lesnek et al., 2018), are broadly synchronous with previously published ice retreat chronologies for the marine-terminating CIS margin elsewhere along the northeast Pacific

500   Coast. However, while our chronology only documents deglaciation, it provides further evidence of a delayed lLGM across the coastal CIS compared to the gLGM maximum extents of alpine glaciers in mainland Alaska (Briner et al., 2017), parts of southern Alaska (Reger et al., 1996), and the LIS (Dalton et al., 2020).

505   **5.5 Paleoclimate Records from the North Pacific**

Several paleoclimate records from around the North Pacific span our interval of CIS deglaciation in the Alexander Archipelago. A combined diatom assemblage- and alkenone-derived record of sea surface temperatures (SSTs) from the Bering Sea (Core 51JPC), records perennial sea ice

510   from ~22.5 ka (beginning of record) to 17 ka, and increased SSTs beginning ~16.9 ka before a notable shift back to annual sea ice ~16.7 ka (Caissie et al., 2010). In the northern Gulf of Alaska (Core EW0408-85JC), $\delta^{18}O$ data document increasing SSTs at 16.7 ka and again at ~14.7 ka (Davies et al., 2011). Alkenone-inferred paleo-SST reconstructions from this same core show the lowest SSTs (~5°C) circa 17.0 ka, with increased SSTs beginning ~16.5 ka, and a rapid ~3-4 °C

515   rise in SSTs from 15.2 to 14.7 ka (Praetorius et al., 2015). Alkenone-inferred SST and $\delta^{18}O$ records from the Gulf of Alaska also record increased SSTs of ~3°C at 14.7 ka (cores EW0408-

26JC, EW0408-66JC; Praetorius et al., 2016). Off Vancouver Island, Mg/Ca temperature

reconstructions from subsurface-dwelling *N. pachyderma* indicate two stages of warming of 2°C

at 17.2 – 16 ka, and 15.5 – 14.0 ka, while surface-dwelling *G. bulloides* record a 3°C SST

520   increase from 15.0 – 14.0 ka (core MD02-2496; Taylor et al., 2014), all within uncertainty of

coastal Alexander Archipelago ice retreat. Alkenone SST reconstructions from another nearby

core (core JT96-09) also indicates a 4°C increase in SST at ~14.7 ka (Kienast and McKay,

2001).

        There are few terrestrial paleoclimate data that span the last deglacial period from SE AK

525   and coastal British Columbia. Cordilleran ice cover until ~15 ka across much of the region

impeded the preservation of many terrestrial records – however, there are limited ice core,

speleothem, and lake records that date back to early regional deglaciation or prior. Fisher et al.

(2008) developed an ice core record from Mt. Logan, British Columbia. However, measurements

of $\delta^{18}O$ likely represent shifting precipitation sources, rather than paleoclimate changes. A

530   growth hiatus in a speleothem from El Capitan Cave (southern Alexander Archipelago) spanning

~41.5 to ~13.4 ka suggests the cave was either overridden by the CIS, experienced permafrost

conditions and a mean annual air temperature < 0°C, or lacked drip water (Wilcox et al., 2019).

However, El Capitan Cave is ~60 km inland of the outermost coastal region and therefore may

have still experienced these conditions while the outer coast deglaciated. At Hummingbird Lake,

535   southwestern Baranof Island, pollen records indicate *Pinus contorta* dominated from ~15.2 ka to

14 ka, which is interpreted to represent *Pinus contorta* response to the beginnings of Gulf of

Alaska ocean warming at ~16.5 ka (Praetorius et al., 2015; Ager, 2019). This record suggests

increased air temperatures around deglaciation of the Alexander Archipelago between 16.3 ± 0.8

ka and 15.1 ± 0.9 ka

540 **5.6 Implications for early human migration**

Several studies have focused on scrutinizing potential areas of lLGM glacial refugia in the Alexander Archipelago through a human migration perspective (Carrara et al., 2007; Lesnek et al., 2018), building off similar approaches from elsewhere in the North Pacific (e.g., Warner et

545 al., 1982; Mann and Peteet, 1994; Misarti et al., 2012). Our study focused on southern Baranof and Kruzof islands because previous mapping suggested that parts of these areas were ice-free throughout the lLGM (Carrara et al., 2003; Carrara et al., 2007). However, our [10]Be ages from southern Baranof Island indicate these areas were glaciated throughout the lLGM and not available for human habitation between ~20 ka and ~15.4 ka. Our exposure ages from Kruzof

550 Island also suggest that this area was not ice free until ~14.8 ka.

These results indicate that some of the last major unevaluated areas of possible refugia that are presently above sea-level were covered by ice during the lLGM. At its maximum extent, ice likely extended onto the then-exposed continental shelf. Ice occupation of the continental shelf – or at least parts of the shelf – off the Alexander Archipelago was relatively brief, from

555 ~20.0 to ~16.0 ka (Lesnek et al., 2018). Lowered global sea levels indicate the shelf would have been above contemporary sea level during this time and until ~11 – 8 ka, when sea level neared modern levels in the Alexander Archipelago (Baichtal et al., in press). At a minimum, ice lobes would have existed within the major shelf troughs (e.g., Chatham Strait), likely crossing the entire shelf at these locations; at a maximum, the whole continental shelf may have been

560 occupied by ice from ~20 to ~16 ka. Whether portions of the shelf remained ice-free during the lLGM is unknown, but it is possible. Based on the immediate colonization of *Pinus* at 15.2 ka in Hummingbird Lake, and as early as ~15.4 ka on Pleasant Island, there were likely ice-free areas on the shelf throughout the lLGM (Hansen and Engstrom, 1996; Ager, 2019).

6 Conclusions

565

We conclude that several areas in SE AK previously mapped as ice-free through the lLGM were

covered by ice until between ~16.3 and ~15.1 ka. [10]Be ages from boulders suggest that the

northern coastal Alexander Archipelago deglaciated at 15.1 ± 0.9 ka ,while [10]Be and [36]Cl ages

date ice retreat in the southern portion at 16.3 ± 0.8 ka, following a lLGM that begin after ~20 ka

570   (Lesnek et al., 2018; Lesnek et al., 2020) The timing of deglaciation in the Alexander

Archipelago is similar to some other sites around the CIS coastal margin (e.g., Mann and Peteet,

1994; Misarti et al., 2012), but later than other locations (e.g., Darvill et al., 2018). Notably, the

deglaciation in SE AK is later than in mainland Alaska and Kodiak and Sanak Islands, Alaska,

where records are more aligned with the gLGM. The timing of deglaciation in the Alexander

575   Archipelago is broadly synchronous with regional records of local ocean and air temperature

increases. We also found that anomalously old [10]Be ages of bedrock surfaces are due to

inheritance caused by insufficient ice sheet erosion, and thus, we caution using ages from

bedrock surfaces as direct constraints on ice retreat without additional boulder ages along the

coastal margins of the CIS.

580   Our data indicate that previous mapping of the coastal CIS can be spatially and

temporally improved. We suggest that ice likely extended out on the continental shelf along the

Alexander Archipelago. We are increasingly confident that areas of the coastal CIS mapped as

ice-free throughout the lLGM were in fact covered by ice, and that refugia, if any, would have

been located on the exposed continental shelf. Although more logistically challenging,

585   subsequent studies should evaluate the existence of lLGM refugia in the Alexander Archipelago

by focusing on the previously exposed continental shelf. Special attention should be given to the

northern Alexander Archipelago where ice masses were fed by local ice caps and thus may not

have been as extensive, as opposed to elsewhere in the northeastern Pacific where ice was

sourced from the main body of the CIS.

590

7 Acknowledgements

We acknowledge that these samples were collected on the ancestral lands of the Tlingit and that

the University at Buffalo exists on the land of the Seneca. These peoples are the traditional

595   caretakers of these lands and we give thanks for the opportunity to exist and work on lands that

are rightfully theirs. We thank the Tongass National Forest for assistance with permitting and

logistics. We thank Corey Krabbenhoft, Joseph Tulenko and Karlee Prince for field assistance

and Joseph Tulenko and Chris Sbarra for lab assistance. We also thank PRIME Lab for ^{10}Be

measurements and Lawrence Livermore National Laboratory for ^{36}Cl measurements. This

600   research was funded by NSF (award # 1854550), the National Geographic Society (award #

57989R-19), a Geological Society of America Student Research Grant (grant number 13631)

funded by NSF (award # 1949901), the Alaska Geological Society, and the Mark Diamond

Research Fund of the Graduate Student Association at the University at Buffalo, the State

University of New York.

605

610 **8 References**

Addison, J. A., Beget, J. E., Ager, T. A., and Finney, B. P.: Marine tephrochronology of the Mt. Edgecumbe volcanic field, southeast Alaska, USA, Quaternary Research, 73, 277-292, 2010.

615 Ager, T. A.: Late Quaternary vegetation development following deglaciation of northwestern Alexander Archipelago, Alaska, Frontiers in Earth Science, 7, 104, 2019.

Baichtal, J. F., Lesnek, A. J., Carlson, R. J., Schmuck, N., Smith, J. L., Landwehr, D. J., and Briner, J. P.: Late Pleistocene and Early Holocene Sea level History Glacial Retreat Interpreted from Shell-bearing Marine Deposits of Southeastern Alaska, GSA Geosphere,
620 in press.

Balco, G., Stone, J. O., Lifton, N. A., and Dunai, T. J.: A complete and easily accessible means of calculating surface exposure ages or erosion rates from 10Be and 26Al measurements, Quaternary Geochronology, 3, 174-195, https://doi.org/10.1016/j.quageo.2007.12.001, 2008.

625 Balco, G.: Production rate calculations for cosmic-ray-muon-produced 10Be and 26Al benchmarked against geological calibration data, Quaternary Geochronology, 39, 150-173, 2017.

Barrie, J. V., and Conway, K. W.: Late Quaternary glaciation and postglacial stratigraphy of the northern Pacific margin of Canada, Quaternary Research, 51, 113-123, 1999.

630 Begét, James E., and Roman J. Motyka. "New dates on late Pleistocene dacitic tephra from the Mount Edgecumbe volcanic field, southeastern Alaska." Quaternary Research 49.1 (1998): 123-125.

Blaise, B., Clague, J. J., and Mathewes, R. W.: Time of maximum Late Wisconsin glaciation, West Coast of Canada, Quaternary Research, 34, 282-295, https://doi.org/10.1016/0033-
635 5894(90)90041-I, 1990.

Booth, D. B., Troost, K. G., Clague, J. J., and Waitt, R. B.: The Cordilleran ice sheet, Developments in Quaternary Sciences, 1, 17-43, 2003.

Borchers, B., Marrero, S., Balco, G., Caffee, M., Goehring, B., Lifton, N., Nishiizumi, K., Phillips, F., Schaefer, J., and Stone, J. J. Q. G.: Geological calibration of spallation
640 production rates in the CRONUS-Earth project, 31, 188-198, 2016.

Brew, David A.: Geologic map of the Craig, Dixon Entrance, and parts of the Ketchikan and Prince Rupert quadrangles, Southeastern Alaska, No. 95-215, 1995.

Briner, J. P., and Swanson, T. W.: Using inherited cosmogenic 36Cl to constrain glacial erosion rates of the Cordilleran ice sheet, Geology, 26, 3-6, 1998.

645 Briner, J. P., Tulenko, J. P., Kaufman, D. S., Young, N. E., Baichtal, J. F., and Lesnek, A.: The last deglaciation of Alaska, Cuadernos de investigación geográfica/Geographical Research Letters, 429-448, 2017.

Caissie, B. E., Brigham-Grette, J., Lawrence, K. T., Herbert, T. D., and Cook, M. S.: Last Glacial Maximum to Holocene sea surface conditions at Umnak Plateau, Bering Sea, as inferred
650 from diatom, alkenone, and stable isotope records, Paleoceanography, 25, 2010.

Capps, S. R.: Glaciation in Alaska2330-7102, 1932.

Carrara, P. E., Ager, T. A., Baichtal, J. F., and VanSistine, D. P.: Map of glacial limits and possible refugia in the southern Alexander Archipelago, Alaska, during the late Wisconsin glaciation, Report 2424, 2003.

655   Carrara, P. E., Ager, T. A., and Baichtal, J. F.: Possible refugia in the Alexander Archipelago of
            southeastern Alaska during the late Wisconsin glaciation, Canadian Journal of Earth
            Sciences, 44, 229-244, 10.1139/e06-081, 2007.
        Clague, J. J., Armstrong, J. E., and Mathews, W. H.: Advance of the late Wisconsin Cordilleran
            Ice Sheet in southern British Columbia since 22,000 Yr B.P, Quaternary Research, 13,
660   322-326, https://doi.org/10.1016/0033-5894(80)90060-5, 1980.
        Cook, J. A., Bidlack, A. L., Conroy, C. J., Demboski, J. R., Fleming, M. A., Runck, A. M.,
            Stone, K. D., and MacDonald, S. O.: A phylogeographic perspective on endemism in the
            Alexander Archipelago of southeast Alaska, Biological Conservation, 97, 215-227,
            https://doi.org/10.1016/S0006-3207(00)00114-2, 2001.
665   Corbett, L. B., Bierman, P. R., and Rood, D. H.: An approach for optimizing in situ cosmogenic
            10Be sample preparation, Quaternary Geochronology, 33, 24-34,
            https://doi.org/10.1016/j.quageo.2016.02.001, 2016.
        Cosma, T. N., Hendy, I. L., and Chang, A. S.: Chronological constraints on Cordilleran Ice Sheet
            glaciomarine sedimentation from core MD02-2496 off Vancouver Island (western
670   Canada), Quaternary Science Reviews, 27, 941-955,
            https://doi.org/10.1016/j.quascirev.2008.01.013, 2008.
        Dalton, A. S., Margold, M., Stokes, C. R., Tarasov, L., Dyke, A. S., Adams, R. S., Allard, S.,
            Arends, H. E., Atkinson, N., and Attig, J. W.: An updated radiocarbon-based ice margin
            chronology for the last deglaciation of the North American Ice Sheet Complex,
675   Quaternary Science Reviews, 234, 106223, 2020.
        Darvill, C. M., Menounos, B., Goehring, B. M., Lian, O. B., and Caffee, M. W.: Retreat of the
            western Cordilleran ice sheet margin during the last deglaciation, Geophysical Research
            Letters, 45, 9710-9720, 2018.
        Davies, M. H., Mix, A. C., Stoner, J. S., Addison, J. A., Jaeger, J., Finney, B., and Wiest, J.: The
680   deglacial transition on the southeastern Alaska Margin: Meltwater input, sea level rise,
            marine productivity, and sedimentary anoxia, Palaeogeography and Palaeoclimatology,
            26, 10.1029/2010pa002051, 2011.
        Demboski, J. R., Stone, K. D., and Cook, J. A.: FURTHER PERSPECTIVES ON THE HAIDA
            GWAII GLACIAL REFUGIUM, Evolution, 53, 2008-2012, 10.1111/j.1558-
685   5646.1999.tb04584.x, 1999.
        Dyke, A. S.: An outline of North American deglaciation with emphasis on central and northern
            Canada, Developments in quaternary sciences, 2, 373-424, 2004.
        Eberlein, G. D., Churkin, M., Carter, C., Berg, H., and Ovenshine, A.: Geology of the Craig
            quadrangle, Alaska, US Geological Survey, 2331-1258, 1983.
690   Fisher, D., Osterberg, E., Dyke, A., Dahl-Jensen, D., Demuth, M., Zdanowicz, C., Bourgeois, J.,
            Koerner, R. M., Mayewski, P., and Wake, C.: The Mt Logan Holocene—late
            Wisconsinan isotope record: tropical Pacific—Yukon connections, The Holocene, 18,
            667-677, 2008.
        Gregoire, L. J., Otto-Bliesner, B., Valdes, P. J., and Ivanovic, R.: Abrupt Bølling warming and
695   ice saddle collapse contributions to the Meltwater Pulse 1a rapid sea level rise,
            Geophysical research letters, 43, 9130-9137, 2016.
        Hansen, B. C. S., and Engstrom, D. R.: Vegetation history of Pleasant Island, southeastern
            Alaska, since 13,000 yr BP, Quaternary Research, 46, 161-175, 1996.

Ivanovic, R. F., Gregoire, L. J., Wickert, A. D., Valdes, P. J., and Burke, A.: Collapse of the North American ice saddle 14,500 years ago caused widespread cooling and reduced ocean overturning circulation, Geophysical Research Letters, 44, 383-392, 2017.

Jones, R. S., Whitehouse, P. L., Bentley, M. J., Small, D., and Dalton, A. S.: Impact of glacial isostatic adjustment on cosmogenic surface-exposure dating, Quaternary Science Reviews, 212, 206-212, 2019.

Kienast, S. S., and McKay, J. L.: Sea surface temperatures in the subarctic northeast Pacific reflect millennial-scale climate oscillations during the last 16 kyrs, Geophysical Research Letters, 28, 1563-1566, 2001.

Lal, D.: Cosmic ray labeling of erosion surfaces: in situ nuclide production rates and erosion models, Earth and Planetary Science Letters, 104, 424-439, 1991.

Lesnek, A. J., Briner, J. P., Lindqvist, C., Baichtal, J. F., and Heaton, T. H.: Deglaciation of the Pacific coastal corridor directly preceded the human colonization of the Americas, Science Advances, 4, eaar5040, 10.1126/sciadv.aar5040 %J Science Advances, 2018.

Lesnek, A. J., Briner, J. P., Baichtal, J. F., and Lyles, A. S.: New constraints on the last deglaciation of the Cordilleran Ice Sheet in coastal Southeast Alaska, Quaternary Research, 96, 140-160, 2020.

Maier, E., Zhang, X., Abelmann, A., Gersonde, R., Mulitza, S., Werner, M., Méheust, M., Ren, J., Chapligin, B., and Meyer, H.: North Pacific freshwater events linked to changes in glacial ocean circulation, Nature, 559, 241-245, 2018.

Mann, D. H.: Wisconsin and Holocene glaciation of southeast Alaska, 1986.

Mann, D. H., and Peteet, D. M.: Extent and Timing of the Last Glacial Maximum in Southwestern Alaska, Quaternary Research, 42, 136-148, https://doi.org/10.1006/qres.1994.1063, 1994.

Mann, D. H., and Hamilton, T. D.: Late Pleistocene and Holocene Paleoenvironments of the Pacific Coast, Quaternary Science Reviews, 14, 449-471, 10.1016/0277-3791(95)00016-i, 1995.

Marrero, S. M., Phillips, F. M., Borchers, B., Lifton, N., Aumer, R.,and Balco, G: Cosmogenic nuclide systematics and the CRONUScalc program, Quaternary Geochronology, 31, 160-187, 2016a.

Marrero, S.M., Phillips, F.M., Caffee, M.W. and Gosse, J.C.,: CRONUS-Earth cosmogenic ^{36}Cl calibration. Quaternary Geochronology, 31, 199-219, 2016b.

Mathewes, R. W., and Clague, J. J.: Paleoecology and ice limits of the early Fraser glaciation (Marine Isotope Stage 2) on Haida Gwaii, British Columbia, Canada, Quaternary Research, 88, 277-292, 10.1017/qua.2017.36, 2017.

Miller, R. D.: Gastineau channel formation: a composite glaciomarine deposit near Juneau, Alaska, US Government Printing Office, 1973.

Misarti, N., Finney, B. P., Jordan, J. W., Maschner, H. D. G., Addison, J. A., Shapley, M. D., Krumhardt, A., and Beget, J. E.: Early retreat of the Alaska Peninsula Glacier Complex and the implications for coastal migrations of First Americans, Quaternary Science Reviews, 48, 1-6, https://doi.org/10.1016/j.quascirev.2012.05.014, 2012.

Molnia, B. F.: Glaciers of North America-Glaciers of Alaska, Geological Survey (US), 2008.

Nishiizumi, K., Imamura, M., Caffee, M. W., Southon, J. R., Finkel, R. C., and McAninch, J.: Absolute calibration of 10Be AMS standards, Nuclear Instruments and Methods in Physics Research Section B: Beam Interactions with Materials and Atoms, 258, 403-413, https://doi.org/10.1016/j.nimb.2007.01.297, 2007.

745 Porter, S. C., and Swanson, T. W.: Radiocarbon age constraints on rates of advance and retreat of
the Puget lobe of the Cordilleran ice sheet during the last glaciation, Quaternary
Research, 50, 205-213, 1998.

Praetorius, S., Mix, A., Jensen, B., Froese, D., Milne, G., Wolhowe, M., Addison, J., and Prahl,
F.: Interaction between climate, volcanism, and isostatic rebound in Southeast Alaska
750 during the last deglaciation, Earth and Planetary Science Letters, 452, 79-89, 2016.

Praetorius, S. K., and Mix, A. C.: Synchronization of North Pacific and Greenland climates
preceded abrupt deglacial warming, Science, 345, 444-448, 2014.

Praetorius, S. K., Mix, A. C., Walczak, M. H., Wolhowe, M. D., Addison, J. A., and Prahl, F. G.:
North Pacific deglacial hypoxic events linked to abrupt ocean warming, Nature, 527,
755 362-366, 2015.

Reger, R. D., Pinney, D. S., Burke, R. M., and Wiltse, M. A.: Catalog and initial analyses of
geologic data related to middle to late Quaternary deposits, Cook Inlet region, Alaska,
State of Alaska Division of Geological and Geophysical Surveys Report of
Investigations, 95-96, 1996.

760 Riehle, J. R., Brew, D. A., Reed, K. M., and Bartsch-Winkler, S.: Explosive latest Pleistocene (?)
and Holocene activity of the Mount Edgecumbe volcanic field, Alaska, US Geological
Survey Circular, 939, 111-114, 1984.

Riehle, J. R., Champion, D. E., Brew, D. A., and Lanphere, M. A.: Pyroclastic deposits of the
Mount Edgecumbe volcanic field, southeast Alaska: eruptions of a stratified magma
765 chamber, Journal of volcanology and geothermal research, 53, 117-143, 1992.

Riehle, J. R.: The Mount Edgecumbe Volcanic Field: A Geologic History, US Department of
Agriculture, Forest Service, Alaska Region, 1996.

Seguinot, J., Khroulev, C., Rogozhina, I., Stroeven, A. P., and Zhang, Q.: The effect of climate
forcing on numerical simulations of the Cordilleran ice sheet at the Last Glacial
770 Maximum, The Cryosphere, 8, 1087-1103, 2014.

Seguinot, J., Rogozhina, I., Stroeven, A. P., Margold, M., and Kleman, J.: Numerical simulations
of the Cordilleran ice sheet through the last glacial cycle, The Cryosphere, 10, 639-664,
2016.

Shafer, A. B., Cullingham, C. I., Cote, S. D., and Coltman, D. W.: Of glaciers and refugia: a
775 decade of study sheds new light on the phylogeography of northwestern North America,
Mol Ecol, 19, 4589-4621, 10.1111/j.1365-294X.2010.04828.x, 2010.

Shafer, A. B. A., White, K. S., Côté, S. D., and Coltman, D. W.: Deciphering translocations from
relicts in Baranof Island mountain goats: is an endemic genetic lineage at risk?,
Conservation Genetics, 12, 1261-1268, 10.1007/s10592-011-0227-8, 2011.

780 Shakun, J. D., Clark, P. U., He, F., Marcott, S. A., Mix, A. C., Liu, Z., Otto-Bliesner, B.,
Schmittner, A., and Bard, E.: Global warming preceded by increasing carbon dioxide
concentrations during the last deglaciation, Nature, 484, 49-54, 2012.

Spratt, R. M., and Lisiecki, L. E.: A Late Pleistocene sea level stack, Climate of the Past, 12,
1079-1092, 2016.

785 Staiger, J., Gosse, J., Toracinta, R., Oglesby, B., Fastook, J., and Johnson, J. V.: Atmospheric
scaling of cosmogenic nuclide production: climate effect, Journal of Geophysical
Research: Solid Earth, 112, 2007.

Stuiver, M., Reimer, P.J., and Reimer, R.W., CALIB 8.2, http://calib.org, 2021.

Tarasov, L., Dyke, A. S., Neal, R. M., and Peltier, W. R.: A data-calibrated distribution of
790 deglacial chronologies for the North American ice complex from glaciological modeling,

Earth and Planetary Science Letters, 315-316, 30-40,
https://doi.org/10.1016/j.epsl.2011.09.010, 2012.

Taylor, M. A., Hendy, I. L., and Pak, D. K.: Deglacial ocean warming and marine margin retreat
of the Cordilleran Ice Sheet in the North Pacific Ocean, Earth and Planetary Science
795   Letters, 403, 89-98, 10.1016/j.epsl.2014.06.026, 2014.

Warner, B. G., Mathewes, R. W., and Clague, J. J.: Ice-free conditions on the Queen Charlotte
Islands, British Columbia, at the height of late Wisconsin glaciation, Science, 218, 675-
677, 1982.

Wilcox, P. S., Dorale, J. A., Baichtal, J. F., Spotl, C., Fowell, S. J., Edwards, R. L., and Kovarik,
800   J. L.: Millennial-scale glacial climate variability in Southeastern Alaska follows
Dansgaard-Oeschger cyclicity, Sci Rep, 9, 7880, 10.1038/s41598-019-44231-1, 2019.

Wilson, F. H., Hults, C. P., Mull, C. G., and Karl, S. M.: Geologic map of Alaska, US
Department of the Interior, US Geological Survey, 2015.

Young, N. E., Schaefer, J. M., Briner, J. P., and Goehring, B. M.: A [10]Be production-rate
805   calibration for the Arctic, Journal of Quaternary Science, 28, 515-526, 2013.

810

815

820

825   **Figures**
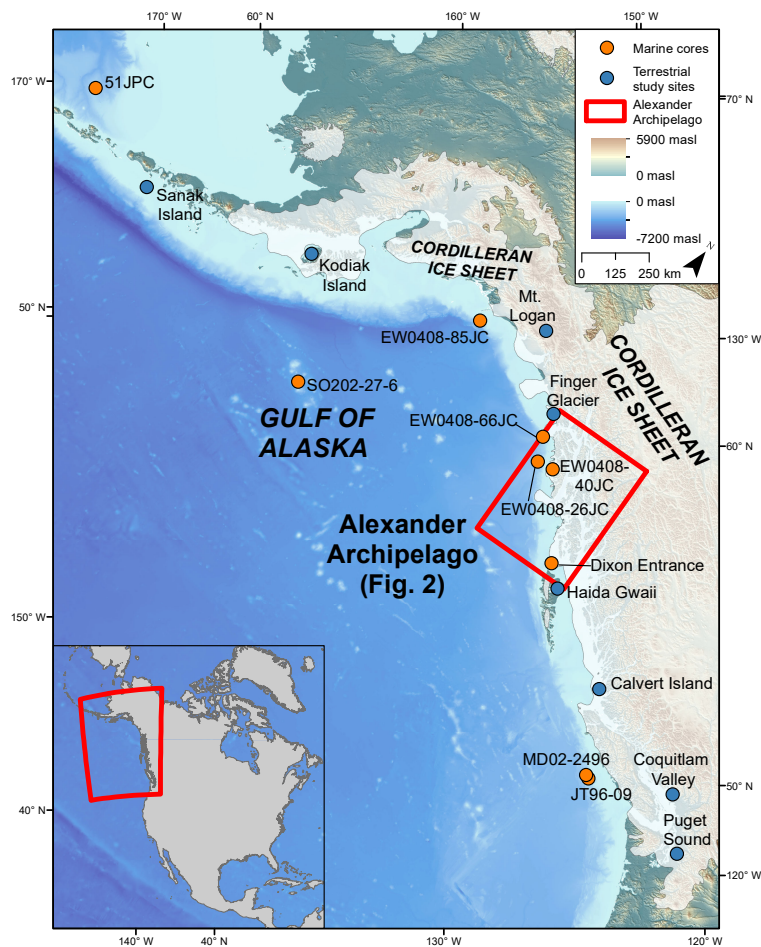
Figure 1: Map of the north Pacific region showing ice limits at 18.0 ka from Dalton et al. (2020) with location of relevant sites mentioned in the text. The Alexander Archipelago is highlighted
830   by the red box. Orange dots indicate locations of marine sediment cores: 51-JPC (Caissie et al., 2010), SO202-27-6 (Maier et al., 2018), EW0408-85JC (Davies et al., 2011; Praetorius and Mix, 2014, Praetoruis et al., 2015), EW0408-66JC (Praetorius and Mix, 2014; Praetorius et al., 2016), EW0408-26JC (Praetorius and Mix, 2014; Praetorius et al., 2016), EW0408-40JC (Addison et al., 2010), MD02-2496 (Cosma and Hendy, 2008), and JT96-09 (Kienast and McKay, 2001).
835   Blue dots indicate location of terrestrial study sites: Sanak Island (Misarti et al., 2012), Kodiak Island (Mann and Peteet, 1994), Mt. Logan (Fisher et al., 2008), Finger Glacier (Mann 1986), Haida Gwaii (Clague et al.,1982; Mathewes and Clague, 1982), Calvert Island, (Darvill et al., 2018), Coquitlam Valley (Clague et al., 1980), and Puget Sound (Porter and Swanson, 1998).
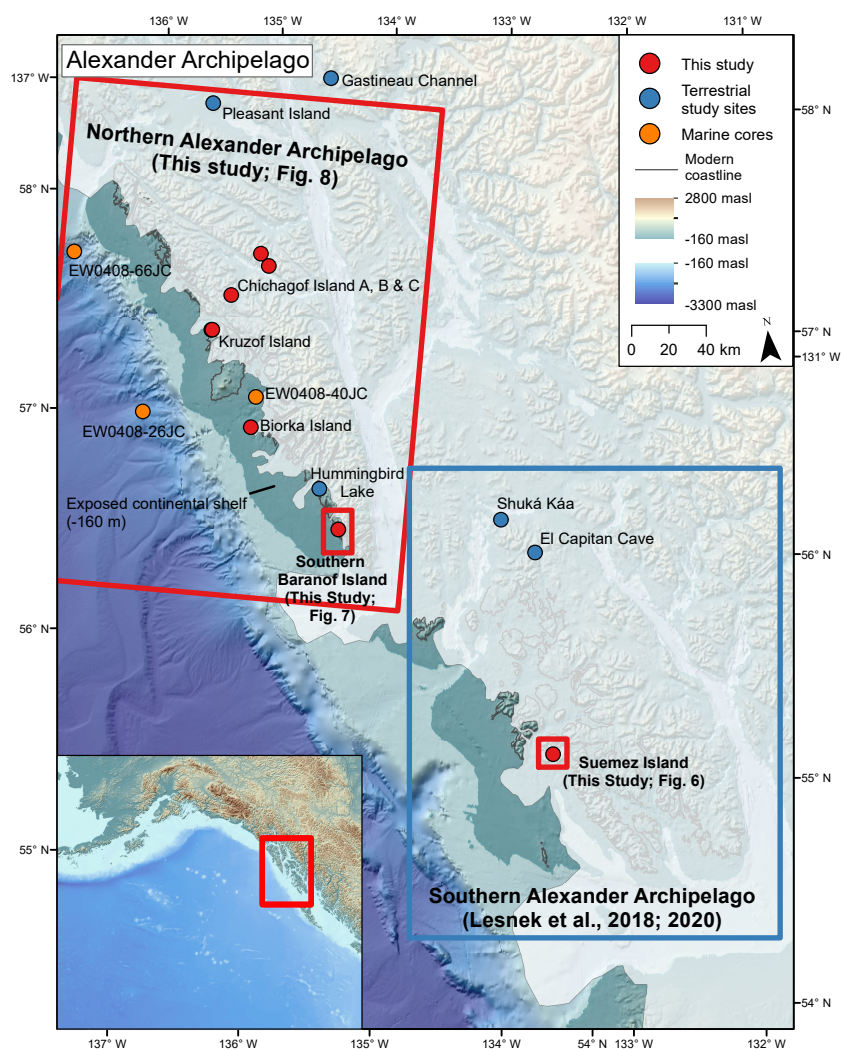
Figure 2: The Alexander Archipelago showing relevant marine sediment cores and terrestrial chronologies. Shaded white areas show hypothesized lLGM CIS extent (Lesnek et al., 2020). -160 m relative sea level lowering after Baichtal et al. (in press). Red boxes and points show sampling locations from this study. Blue box shows extent of study area from Lesnek et al. (2018; 2020). Orange dots represent locations of marine sediment cores: EW0408-66JC and EW0408-26J (Praetorius and Mix, 2014; Praetorius et al., 2016) and EW0408-40JC (Addison et al., 2010). Blue dots indicate locations of relevant terrestrial study sites: Gastineau Channel (Miller, 1973), Pleasant Island (Hansen and Engstrom, 1996), Hummingbird Lake (Ager, 2019), Shuká Káa (Lesnek et al., 2018), and El Capitan Cave (Wilcox et al., 2019).
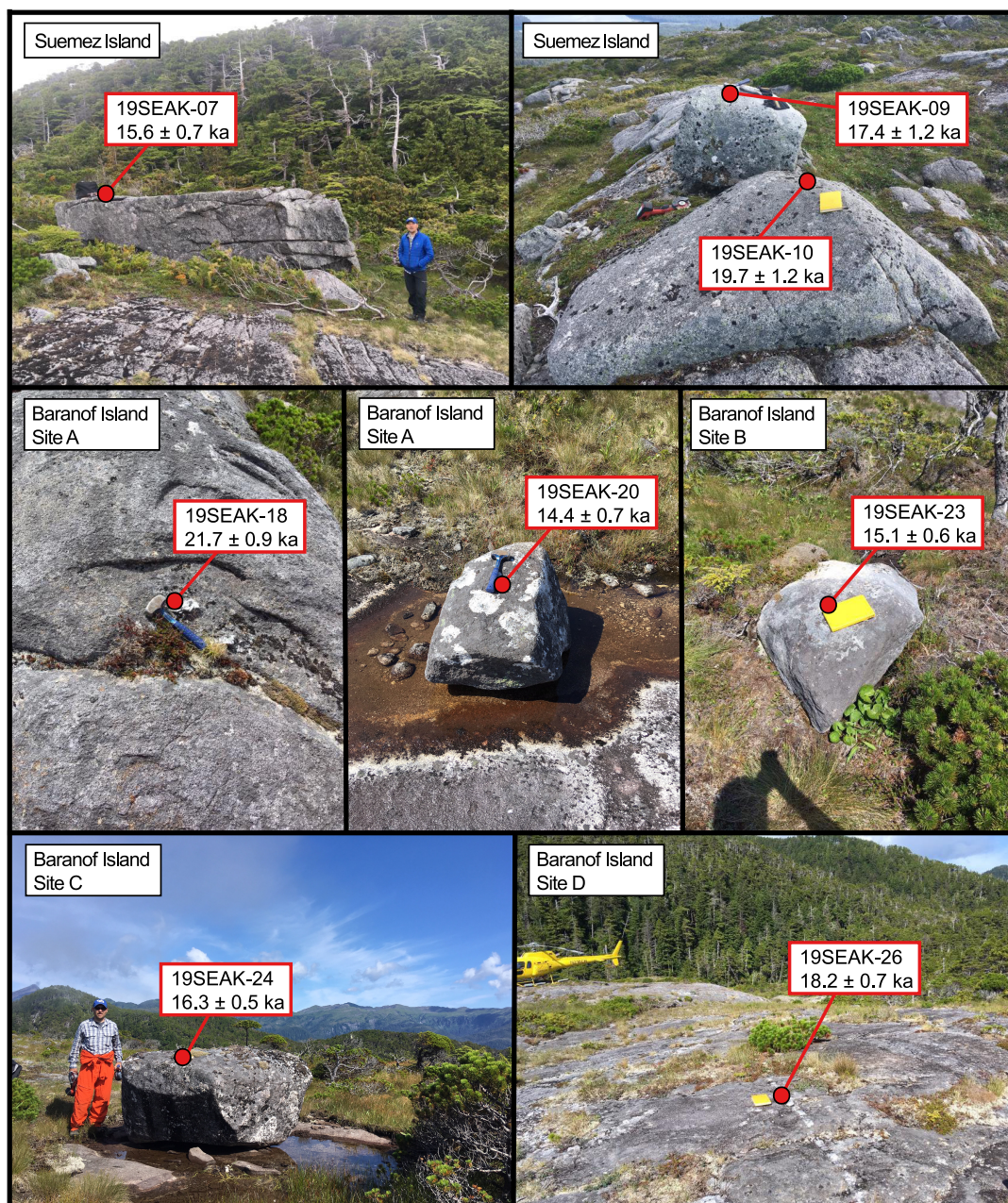
Figure 3: Sample photos from 2019 field season. All ^{10}Be ages shown with 1 σ internal uncertainty. Note the grooves and chatter marks on bedrock of 19SEAK-18.

Figure 4: Sample photos from 2018 and 2020 field season. All [10]Be ages are shown with 1 σ internal uncertainty. Note the relatively small size of 20SEAK-15.
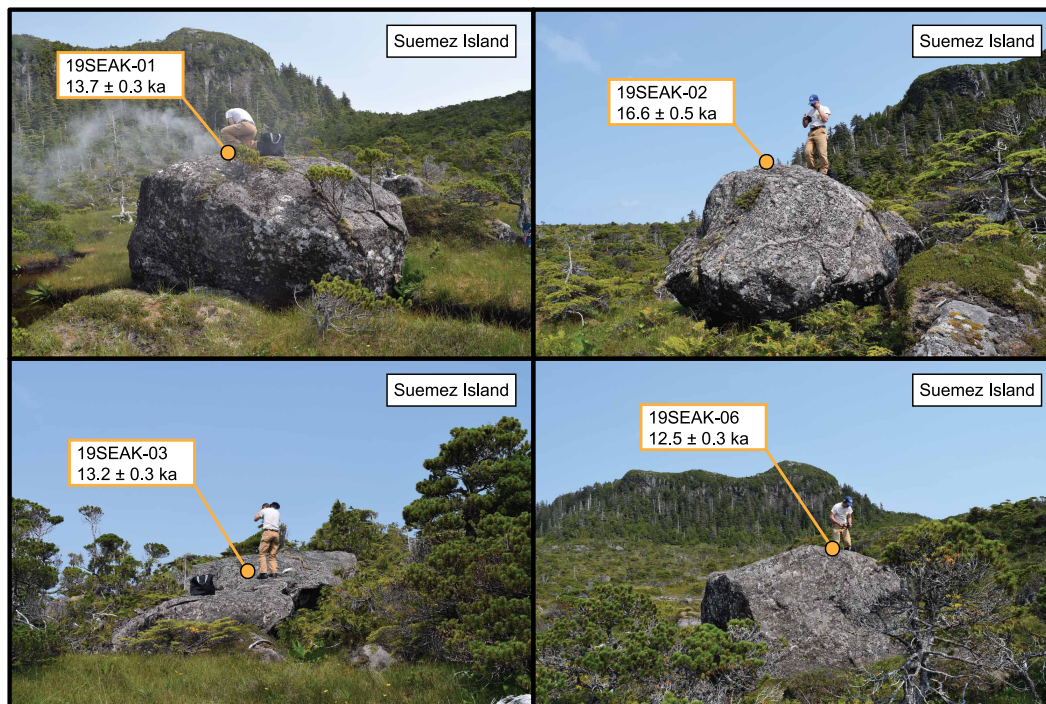
855

Figure 5: Basalt samples and ^{36}Cl ages from southwestern Suemez Island. Ages are reported at 1 σ internal uncertainty.

860

865

870   Table 1: [10]Be surface exposure age data.

Sample ID	Sample type	Latitude (°N)[a]	Longitude (°W)[a]	Elevation (m asl)[a]	Sample thickness (cm)	Topographic shielding correction	Quartz (g)	[9]Be added (µg)	[10]Be/[9]Be ratio[b]	[10]Be/[9]Be ratio uncertainty	[10]Be (atoms/g)	[10]Be uncertainty (atoms/g)	[10]Be age (ka) Arctic PR	[10]Be age (ka) Global PR
BIORKA ISLAND														
18JB005	Boulder	56.8482	-135.5314	47	3.0	1.0000	34.37	232	1.36E-13	4.38E-15	6.60E+04	2.12E+03	15.3 ± 0.5	14.7 ± 0.5
18JB006	Boulder	56.8471	-135.5315	43	3.0	1.0000	34.57	221	1.32E-13	4.87E-15	6.40E+04	2.35E+03	14.9 ± 0.6	14.3 ± 0.5
18JB007	Boulder	56.8527	-135.5363	46	3.0	1.0000	33.92	233	1.35E-13	4.54E-15	6.60E+04	2.23E+03	15.4 ± 0.5	14.8 ± 0.5
18JB008	Boulder	56.8528	-135.5362	46	3.0	1.0000	24.35	232	8.60E-14	2.92E-15	5.90E+04	1.99E+03	13.7 ± 0.5	13.2 ± 0.4
SUEMEZ ISLAND														
19SEAK-07	Boulder	55.2469	-133.3414	376	2.0	0.9958	21.24	233	1.25E-13	5.41E-15	9.19E+04	3.97E+03	15.6 ± 0.7	14.9 ± 0.6
19SEAK-08	Boulder	55.2470	-133.3419	392	2.0	0.9984	12.04	226	7.20E-14	5.42E-15	9.03E+04	6.80E+03	15.0 ± 1.1	14.4 ± 1.1
19SEAK-09	Boulder	55.2477	-133.3406	394	2.0	1.0000	19.44	233	1.31E-13	9.28E-15	1.05E+05	7.44E+03	17.4 ± 1.2	16.7 ± 1.2
19SEAK-10	Bedrock	55.2477	-133.3406	419	3.0	1.0000	17.81	213	1.38E-13	8.63E-15	1.21E+05	7.55E+03	19.7 ± 1.2	18.9 ± 1.2
BARANOF ISLAND														
Site A														
19SEAK-17	Boulder	55.3677	-134.9015	140	2.0	0.9923	25.08	233	1.30E-13	6.21E-15	8.02E+04	3.84E+03	16.9 ± 0.8	16.3 ± 0.8
19SEAK-18	Bedrock	56.3723	-134.9084	129	2.0	1.0000	25.24	232	1.66E-13	6.95E-15	1.02E+05	4.27E+03	21.7 ± 0.9	20.8 ± 0.9
19SEAK-19	Bedrock	56.3718	-134.9094	126	2.0	1.0000	24.80	233	2.10E-13	8.06E-15	1.31E+05	5.05E+03	28.0 ± 1.1	26.9 ± 1
19SEAK-20	Boulder	56.3712	-134.9082	135	2.0	1.0000	25.03	233	1.09E-13	5.59E-15	6.80E+04	3.47E+03	14.4 ± 0.7	13.8 ± 0.7
Site B														
19SEAK-21	Boulder	56.3636	-134.9068	48	2.0	1.0000	25.05	233	1.00E-13	4.57E-15	6.23E+04	2.84E+04	14.4 ± 0.7	13.8 ± 0.6
19SEAK-22	Bedrock	56.3636	-134.9072	58	2.0	0.9749	20.17	230	8.03E-14	3.10E-15	6.13E+04	2.36E+03	14.4 ± 0.6	13.8 ± 0.5
19SEAK-23	Boulder	56.3638	-134.9092	68	2.0	0.9911	20.24	231	8.64E-14	3.29E-15	6.60E+04	2.51E+03	15.1 ± 0.6	14.5 ± 0.6
Site C														
19SEAK-24	Boulder	56.3228	-134.892	150	1.5	1.0000	20.12	234	1.01E-13	3.39E-15	7.83E+04	2.63E+03	16.3 ± 0.5	15.6 ± 0.5
19SEAK-25	Bedrock	56.3231	-134.8916	163	1.5	1.0000	19.99	234	9.80E-14	3.41E-15	7.68E+04	2.67E+03	15.7 ± 0.6	15.1 ± 0.5
Site D														
19SEAK-26	Bedrock	56.3554	-134.8856	145	2	0.9879	25.12	235	1.37E-13	5.54E-15	8.56E+04	3.47E+03	18.2 ± 0.7	17.4 ± 0.7
19SEAK-27	Bedrock	56.3555	-134.8855	142	1.5	0.9963	25.04	233	1.54E-13	5.89E-15	9.59E+04	3.67E+03	20.2 ± 0.8	19.3 ± 0.7
KRUZOF ISLAND														
20SEAK-7	Boulder	57.3112	-135.8126	558	1.5	0.9976	20.14	233	1.36E-13	7.24E-15	1.05E+05	5.59E+03	14.9 ± 0.8	14.3 ± 0.8
20SEAK-10	Bedrock	57.3112	-135.8111	559	1.5	0.96912	20.13	231	1.20E-13	8.48E-15	9.23E+04	6.50E+03	13.4 ± 1.0	12.9 ± 0.9
20SEAK-12	Boulder	57.3110	-135.8110	569	1.0	0.9927	20.07	382	8.32E-14	3.74E-15	1.06E+05	4.77E+03	14.9 ± 0.7	14.3 ± 0.6
20SEAK-13	Boulder	57.3109	-135.8109	568.3	1.0	0.9941	20.25	230	1.36E-13	7.43E-15	1.04E+05	5.65E+03	14.6 ± 0.8	14.1 ± 0.8
CHICHAGOF ISLAND														
Site A														
20SEAK-14	Bedrock	57.4621	-135.6554	476	0.5	1.0000	20.25	230	1.34E-13	6.34E-15	1.01E+05	4.80E+03	15.3 ± 0.7	14.6 ± 0.7
20SEAK-15	Boulder	57.4621	-135.6554	476	1.0	1.0000	20.33	227	1.13E-13	6.04E-15	8.38E+04	4.50E+03	12.7 ± 0.7	12.2 ± 0.7
20SEAK-16	Boulder	57.4618	-135.6351	473	1.5	1.0000	20.26	240	7.48E-14	4.78E-15	5.92E+04	3.78E+03	9.0 ± 0.6	8.6 ± 0.6
Site B														
20SEAK-18	Boulder	57.5743	-135.2721	817	3.0	1.0000	15.20	226	1.09E-13	7.99E-15	1.09E+05	7.99E+03	12.4 ± 0.9	11.8 ± 0.9
20SEAK-19	Bedrock	57.5743	-135.2720	816	1.5	1.0000	20.05	239	1.57E-13	7.31E-15	1.25E+05	5.81E+03	14.1 ± 0.7	13.5 ± 0.6
Site C														
20SEAK-22	Bedrock	57.6425	-135.3483	779	2.0	1.0000	20.12	231	1.98E-13	8.58E-15	1.52E+05	6.59E+03	17.7 ± 0.8	17.0 ± 0.7

[a] Elevations and positions were recorded with a Garmin handheld GPS receiver (~5 m vertical uncertainty) or GAIA GPS (~5 m vertical uncertainty)

[b] AMS results from PRIME Lab are standardized to 07KNSTD (Nishiizumi et al., 2007); ratios are blank corrected and shown at 1 SD uncertainty.

[c] [10]Be ages reported with at one σ internal uncertainties and calculated with CRONUS-Earth calculator v. 3 (Balco et al., 2008) using the Arctic production rate (Young et al., 2013) or global production rate (Borchers et al., 2016) and Lm scaling.

Table 2: ^{36}Cl surface exposure age data

Sample ID	Sample type	Latitude (°N)[f]	Longitude (°W)[f]	Elevation (m asl)[f]	Sample thickness (cm)	Density (g/cm³)	Topographic Shielding Correction	Aliquot dissolved (g)	^{37}Cl-enriched spike added (g)[a]	^{35}Cl/^{37}Cl ratio[b]	Rock sample dissolved (g)	Natural Cl carrier added (g)[c]	^{36}Cl/Cl	^{36}Cl/Cl uncertainty[b]	^{36}Cl concentration (atoms/g)[d]	^{36}Cl age (ka)[e]
ROCK SAMPLES																
19SEAK-01[f]	Boulder	55.2449	-133.4328	391	2.5	2.8	0.995658	1.1484	0.0587	1.36E-13	12.0014	0.2493	1.50E-13	3.34E-15	2.33E+03	13.7 ± 0.3
19SEAK-02[f]	Boulder	55.2461	-133.4327	398	3	2.8	0.994066	1.0383	0.0593	1.32E-13	11.5081	0.3027	1.77E-13	5.07E-15	3.69E+03	16.6 ± 0.5
19SEAK-03[g]	Boulder	55.246	-133.4324	398	2.5	2.8	0.994066	1.2061	0.0595	1.35E-13	14.0301	0.1193	2.02E-13	4.30E-15	2.61E+03	13.2 ± 0.3
19SEAK-06[f]	Boulder	55.2448	-133.4355	398	2	2.8	0.995524	1.2081	0.0619	8.60E-14	20.0269	0.219	2.46E-13	5.43E-15	2.29E+03	12.5 ± 0.3
PROCESS BLANKS																
CLBLK-AQ4	-	-	-	-	-	-	-	0.0607	0.953	-	-	-	-	-	-	-
CLBLK-AQ8	-	-	-	-	-	-	-	0.0596	0.936	-	-	-	-	-	-	-
CLBLK-26	-	-	-	-	-	-	-	-	-	-	0.1998	4.92E-15	6.00E-16	-	-	-
CLBLK-AQ4	-	-	-	-	-	-	-	0.0607	0.953	-	-	-	-	-	-	-

[a] The ^{37}Cl-enriched spike was made at Lawrence Livermore National Laboratory. Its Cl concentration is 1285 ppm and its ^{35}Cl/^{37}Cl ratio is 0.93

[b] The natural Cl carrier was made at the University of New Hampshire. Its Cl concentration is 1436 ± 9 ppm and its ^{35}Cl/^{37}Cl ratio is 3.127

[c] Uncertainties on ^{35}Cl/^{37}Cl ratios and ^{36}Cl/Cl ratios and exposure ages represent propagated 1σ analytical uncertainties only

[d] Sample ^{36}Cl concentrations are corrected for ^{36}Cl contributed by process blank CLBLK-26

[e] Exposure ages are presented at 1 σ internal uncertainty; ages were calculated with the CRONUSEarth 36Cl calculator (http://stoneage.ice-d.org/math/Cl36/v3/v3_Cl36_age_in.html) and Lm scaling (Lal, 1991)

[f] Aliquot for stable Cl measurements processed with CLBLK-AQ8

[g] Aliquot for stable Cl measurements processed with CLBLK-AQ4
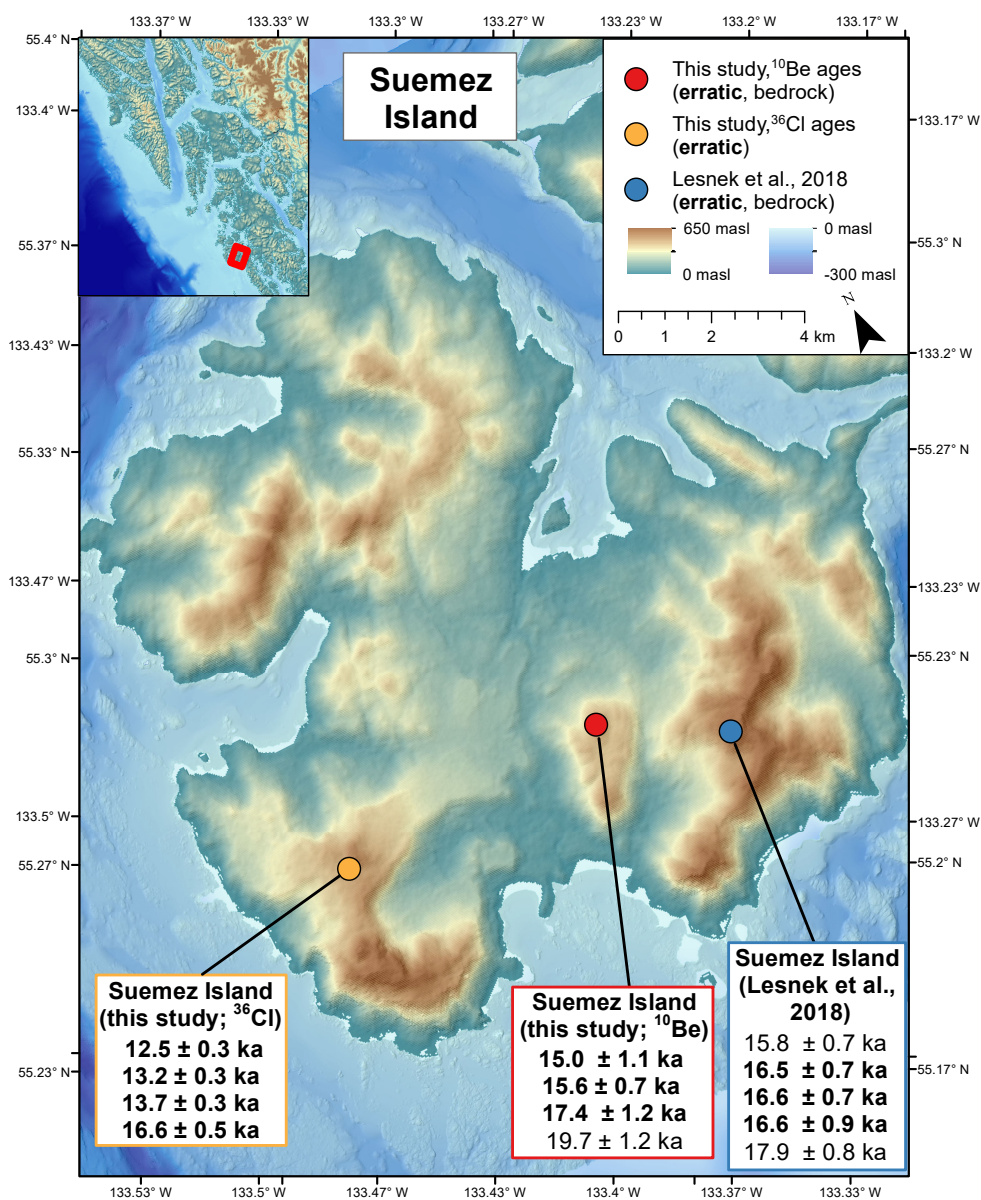
875

Figure 6: ^{10}Be and ^{36}Cl ages from samples collected on Suemez on island: red dot marks sampling site from this study, blue dot marks sampling site from Lesnek et al., 2018). All ^{10}Be and ^{36}Cl ages reported with 1 σ internal uncertainty.
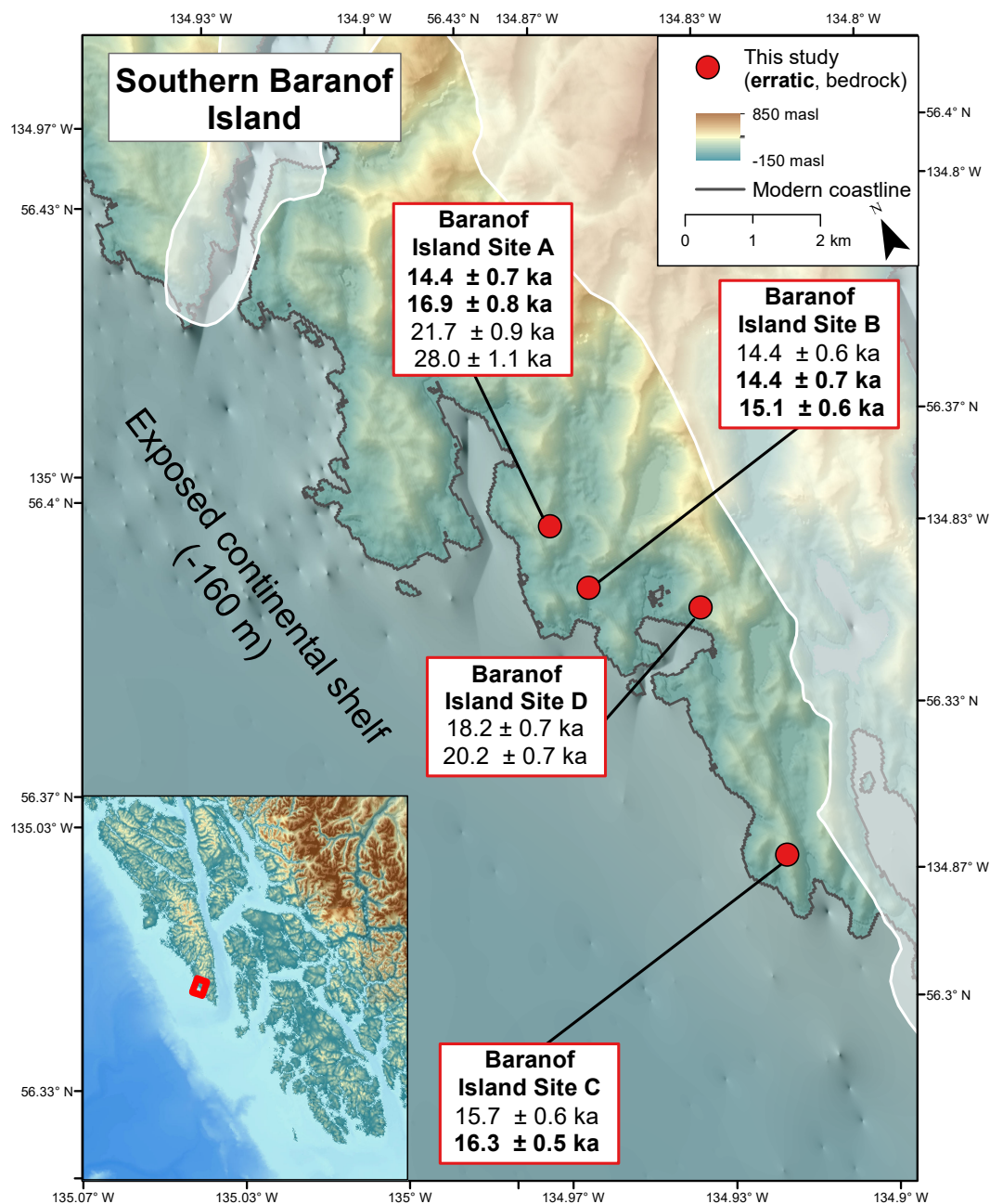
Figure 7: ^{10}Be ages from sampling sites on southern Baranof Island. All ages are reported with 1 σ internal error. CIS lLGM extent after Carrara et al. (2007).
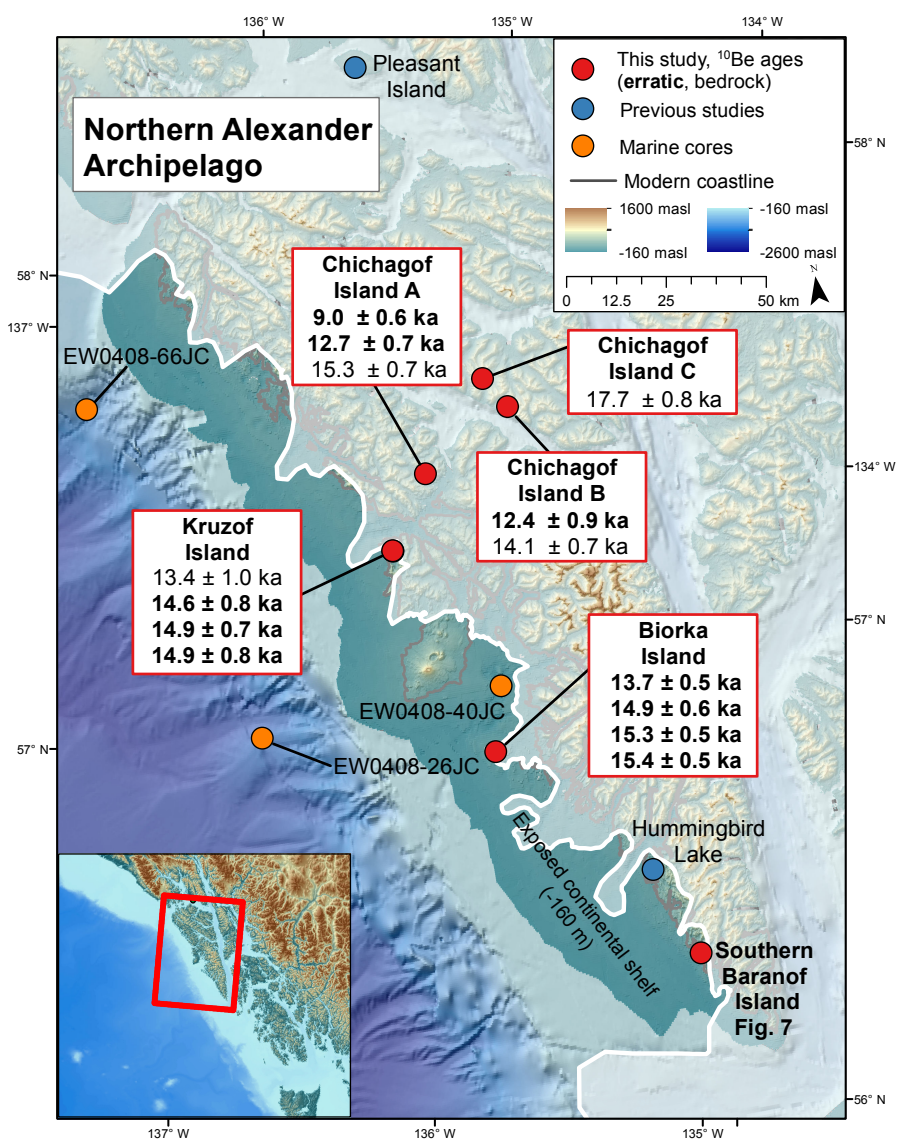
Figure 8: [10]Be ages from sampling sites in the northern Alexander Archipleago. All ages are
reported with 1 σ internal error. lLGM CIS extent after Lesnek et al. (2020). Exposed continental
shelf at -160 m below modern sea level Baichtal et al. (in press). Yellow dots show location of
relevant marine sediment cores: EW0408-66JC and EW0408-26JC (Praetorius and Mix, 2014;
Praetorius et al., 2016) and EW0408-40JC (Addison et al., 2010). Blue dots show locations of
relevant terrestrial study sites: Pleasant Island (Hansen and Engstrom, 1996) and Hummingbird
Lake (Ager, 2019).
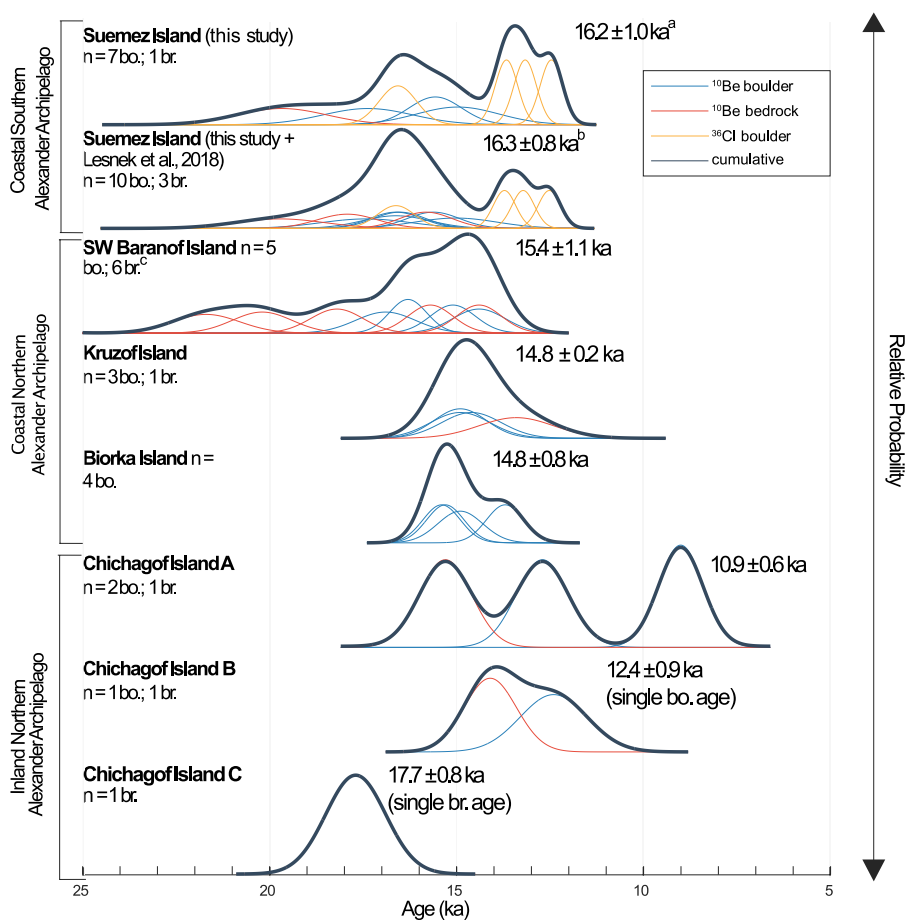
Figure 9: Relative probably plots of bedrock (red) and boulder (blue) ^{10}Be and ^{36}Cl boulder (yellow) ages from this study calculated with 1 σ internal uncertainty. bo. = boulder, br. = bedrock. All ages shown are mean ages from only boulders at each sample site reported with 1 SD unless noted. [a]Average of all ^{10}Be boulder ages and oldest ^{36}Cl boulder age with 1 SD. [b]Average of all ^{10}Be boulder ages (this study and Lesnek et al., 2018) and oldest ^{36}Cl boulder age (this study). [c]One old outlier at 28.0 ± 1.1 ka not shown.

895

900
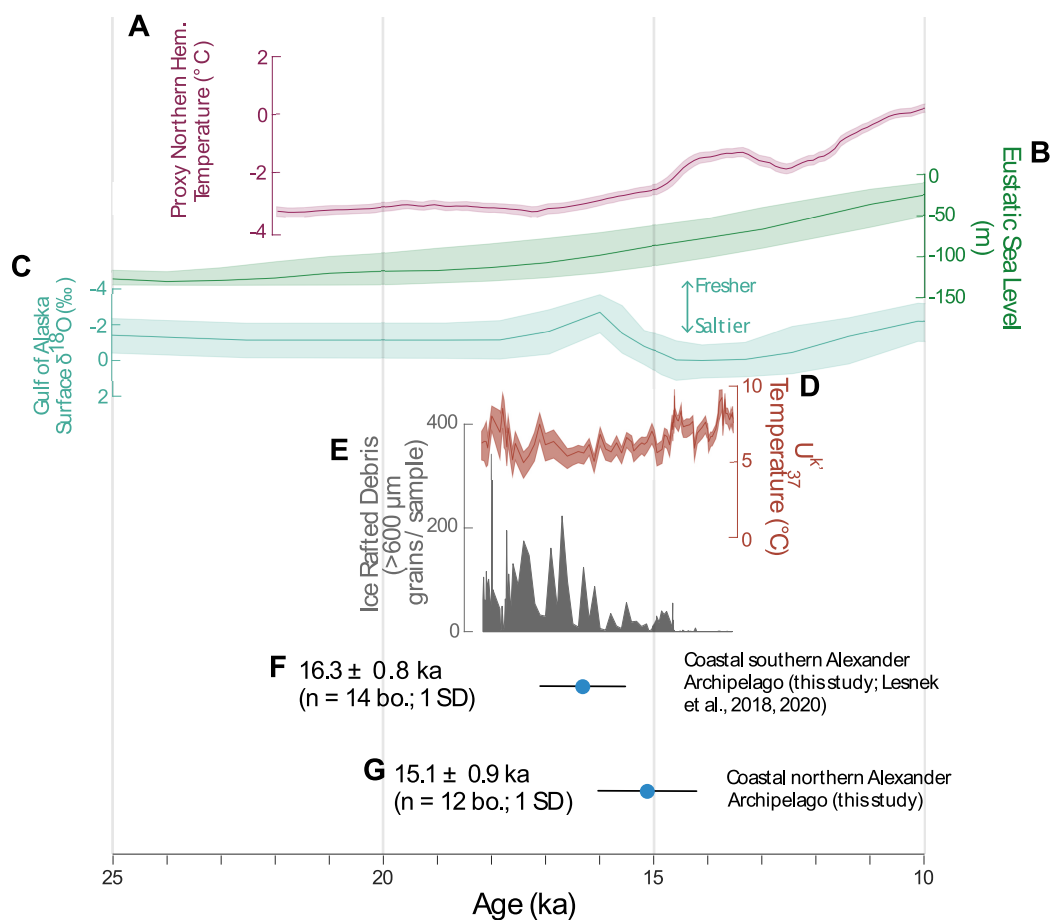
Figure 10: A) Proxy Northern Hemisphere temperature anomaly relative to early Holocene with
1 σ error (Shakun et al., 2012). B) Eustatic sea-level curve (Spratt and Lisiecki, 2016). C) Gulf of
Alaska surface salinity δ^{18}O record (Core SO202-27-6; Maier et al., 2018). D) U$^{K'}_{37}$ temperature
reconstruction from off the coast of the Alexander Archipelago (Cores EW0408-26JC, EW0408-
66JC; Praetorius et al., 2016). E) Ice rafted debris record from off Vancouver Island (Core
MD02-2496; Cosma et al., 2008). F) – G) Relative probability plots of boulder ^{10}Be ages from
the coastal Alexander Archipelago, with mean boulder ages and 1 σ reported (this study; Lesnek
et al., 2018; 2020).